Department of Biosciences and Nutrition,

Karolinska Institutet, Stockholm

Cancer Cell Invasion Laboratory

Investigating the tumor microenvironment of liver metastases

Masterarbeit

Veterinärmedizinische Universität Wien

vorgelegt von

Laura Hermann

Wien, im Monat September 2023

Internal Supervisor: Dr. rer. nat. Sabine Lagger

External Supervisor: Natalie Geyer, PhD

Reviewer: Ao.Univ.-Prof. Mag.rer.nat. Dr.rer.nat.Ingrid Walter

Preface

I do not usually pack my bags before starting a new internship. But this time I did. I had six months to get to know new techniques in the lab, new people and a new country. And although I had to leave my pets behind with a heavy heart, I made the trip to Stockholm to Marco's Cancer Cell Invasion lab.

As they say in German, “klein aber fein” (small but mighty). Marco's group consists of four people without whom my project would not have been possible.

Sara, who not only makes incredibly good ice cream, but also stayed late at times with her helpfulness, allowing me to finish my lab work. On a side note: she is also really good at thawing cells and making sourdough! Annika, with whom I could enjoy every lunch, never shied away from offering her help when I was stuck. Not only did she convince me that Finnish Semla are better than Swedish ones (because they are filled with jam instead of marzipan), but she also searched the lab kitchen and storage rooms with me every time I had forgotten. Marco not only gave me the feeling of trust from the beginning on, he also encouraged me to ask many questions and to look at things critically. One thing is clear: Marco asks the best questions! During Lab meetings or Journal Clubs, I always tried to guess his potential questions, only to be surprised every time. But Marco is not only the question master. From the beginning on he gave me great confidence, encouraged me to believe in myself and also showed me that I am indeed capable of handling tasks even when they are new to me. I have been able to learn a lot from him professionally but also personally.

Lastly, I must mention the person who had to put up with me as a direct work colleague. A big shoutout goes to Natalie who also gave me the feeling of having great confidence in me. Although I was new to this field of research, she gave me the freedom to find out things on my own. Natalie also asks very good questions that hit the mark. Sometimes we both don't know the answer, but you can be sure she knows exactly how to find an answer. And if there is something she doesn't know, she looks it up. With that, she taught me to not be afraid of not knowing the answer to a question and doing experiments for the first time. If something goes wrong then: "ist das jetzt so (denglish translation: is it now so)" , but you do not give up! You quickly notice that she is on fire for her job and she passes that on!

Nevertheless, I am also proud to have at least "taught" her one thing and that is the phrase: "Das geht sich nicht aus!" (Apparently, this is a very Austrian phrase)

And now in all seriousness: Sara, Annika, Marco and Natalie, thank you very much for the valuable experience and the great time. I couldn't have imagined it any better. You are a great team and I felt incredibly comfortable. Stay as you are and keep asking questions!

But before you flip the page to finally find out what I did for the last six months, I want to mentioned one last person. Finalising my thesis would not have been possible without the help of Sabine who is also really good at asking questions. She reminded me of the reality and made me understand that not everyone who reads this thesis has dedicated six months to immersing themselves intensively in this topic every day. I can confidently say that Sabine made sure that this work is of the highest quality (according to our judgment) and she clearly put in every effort to achieve that.

To close this out the only thing that is left to say is: enjoy reading and tack så mycket!

Abstract

The diagnosis of liver metastases dramatically worsens prognosis in patients with gastrointestinal cancer. Histologically, two major growth pattern of liver metastases were described: replacement and encapsulated. Replacement-type metastases are characterized by direct contact between hepatocytes and tumor cells. In encapsulated metastases a fibrotic capsule separates the liver from the tumor. Importantly, encapsulated metastases are linked to improved survival.

Our study explored the role of the tumor microenvironment in pancreatic and colorectal cancer liver metastases (PCLM and CRLM, respectively).

We used multiplex RNA in situ hybridization to characterize the distribution of stromal cells within the capsule of encapsulated CRLM. The results revealed a zonal expression of the fibrotic marker genes *COL1A1, DCN*, *FN1* and *PDGFRA.* In a CRLM cohort including 263 patients pre-operative chemotherapy treatment was associated with a higher degree of encapsulation. Similarly, we show that chemotherapy induces capsule formation in murine CRLM.

In murine replacement-type liver metastases, we detected Stat3 phosphorylation (pStat3) at the invasion front, suggesting activation of the IL-6/JAK/STAT3 signalling axis. Unexpectedly, treatment with IL-6 blocking antibodies did not affect the pStat3 signal. I further established a co-culture system combining hepatocytes and pancreatic cancer cells. Preliminary data indicate that tumor cell addition alone does not induce apoptosis in neighbouring hepatocytes in vitro.

Together, we gave new insights into the process of capsule formation in encapsulated liver metastases and provided evidence that STAT3 signaling is activated in the perimetastatic liver of replacement-type. In summary, our findings provide insights into the complex tumor microenvironment of liver metastases.

Zusammenfassung

Die Diagnose von Lebermetastasen bei Patienten mit gastrointestinalen Tumoren wie Bauchspeicheldrüsen- oder Dickdarmkrebs führt zu einer erheblichen Verschlechterung der Überlebensprognose. Histologisch wurden hauptsächlich zwei Wachstumsmuster von Lebermetastasen beschrieben: „Replacement“ und „Encapsulated“. Aggressive "Replacement"-Metastasen zeigen direkten Zellkontakt zwischen Hepatozyten und Tumorzellen. "Encapsulated"-Metastasen sind von einer fibrotischen Kapsel umgeben. Das „Encapsulated“ Wachstumsmuster ist mit einer besseren Überlebensrate assoziiert.

Ziel unserer Studie war es, die Tumor-Mikroumgebung in Lebermetastasen von Bauchspeicheldrüsen- und Darmkrebs zu untersuchen.

Mittels Multiplex-RNA-in-situ-Hybridisierung konnten wir eine zonale Expression der fibrotischen Markergene *COL1A1, DCN, FN1, PDGFRA* in der Kapsel von kolorektalen Lebermetastasen (KRLM) zeigen. In einer klinischen Kohorte von 263 KRLM Patienten war eine präoperative Chemotherapie mit einem höheren Anteil vom „Encapsulated“-Wachstumsmuster verbunden. Wir konnten diese Ergebnisse in einem Mausmodell bestätigen.

Des Weiteren haben wir Phosphorylierung von Stat3 (pStat3) im perimetastatischen Lebergewebe von murinen Lebermetastasen gezeigt, was auf Aktivierung des IL-6/JAK/STAT3-Signalweges hinweist. Unerwarteterweise hatte die Behandlung von Mäusen mit IL-6 blockierenden Antikörpern keinen Einfluss auf das pStat3-Signal in der perimetastatischen Leber. Im weiteren Verlauf haben ich ein Co-Kultur-System etabliert, mit dem zelluläre Interaktionen zwischen Hepatozyten und Tumorzellen untersucht werden können. Vorläufige Ergebnisse weisen darauf hin, dass das Vorhandensein von Tumorzellen allein keine Apoptose in benachbarten Hepatozyten auslöst.

Zusammenfassend gewannen wir neue Erkenntnisse zur Kapselbildung bei weniger aggressiven Lebermetastasen und zeigten, dass Lebermetastasen vom "Replacement"-Typ durch eine Aktivierung von STAT3 im perimetastatischen Lebergewebe gekennzeichnet sind. Unsere Ergebnisse liefern Einblicke in die komplexe Tumormikroumgebung von Lebermetastasen gastrointestinaler Tumore.

Index

1.Introduction

1.1 Gastrointestinal cancer

Approximately one in four cancer patients are diagnosed with gastrointestinal (GI) cancer, which comprise cancers that originate from the organs of the gastrointestinal tract, such as the colon and the pancreas[1]. In the majority of GI cancer cases, diagnoses are made in advanced stages of the disease, leading to low survival rates. However, this is not entirely applicable to colon cancer, as screening is available and frequently leads to the detection of early stages or precancerous lesions. Metastasis plays a critical role in the poor prognosis of GI cancer. GI cancer liver metastases significantly contribute to cancer-related deaths, with the liver being a major target site for such metastases[2]. Both advanced stages of pancreatic and colorectal cancers often lead to liver metastasis, contributing to worse survival outcomes in patients compared to those without liver metastases[3,4]. Surgical resection is considered the only treatment that can lead to long-term survival in these cases. However, due to late-stage diagnosis and high rates of other distant metastasis, only a small number of patients benefit from this approach[3,4].

1.2 Shedding light on pancreatic cancer: poor survival, aggressive nature and rising incidence

Pancreatic cancer is a highly aggressive disease and the 12th most prevalent type of cancer worldwide[5]. Pancreatic ductal adenocarcinoma (PDAC) is the main histological type of pancreatic cancer, accounting for approximately 90 % of all cases[6]. The five-year overall survival rate of PDAC is 12 %[7] and it is expected to become the second leading cause of cancer-related deaths in the US by 2030, highlighting the urgent need for improved early detection and treatment options [8].

Several risk factors have been linked to an increased risk for PDAC, including long-term cigarette smoking, high-fat and meat diets, obesity, type two diabetes, low serum folate levels, and chronic pancreatitis[9,10].

1.3 Current treatment options for PDAC

To date, the only curative treatment option for PDAC is surgical resection[11]. Different classifications exist to categorize pancreatic cancers as resectable, borderline resectable, or unresectable based on the involvement of adjacent vessels[12]. Resectable tumors have no major vessel invasion, while borderline resectable tumors involve the portal or

superior mesenteric vein but allow for resection and reconstruction[12]. Unresectable tumors invade the superior mesenteric artery or celiac trunk. Imaging techniques such as computerized tomography (CT), magnetic resonance imaging (MRI), positron emission tomography (PET), and endoscopic ultrasound (EUS) are used for detection and staging[12]. If surgery can be carried out, it is usually followed by adjuvant chemotherapy.

However, only about 15 % of patients present with resectable disease at diagnosis, while the remaining 85 % are diagnosed with locally advanced, non-resectable or metastatic disease[11]. Considering the limited therapeutic options for the majority of PDAC patients, the current conventional treatment primarily involves multi-agent palliative chemotherapy due to the high rate of metastases at diagnosis[13]. As a standard treatment, many patients receive Gemcitabine as primary chemotherapeutic agent[13]. The exact mechanism of its action is not completely understood but it is known that Gemcitabine can hinder DNA synthesis, which leads to the formation of DNA damage and ultimately results in programmed cell death[14]. Another possible effect of Gemcitabine is the intercalation into DNA, which leads to the inhibition of both DNA synthesis and repair processes[14]. Gemcitabine was approved by the U.S. Food and Drug Administration (FDA) in 1996 and is successfully used in combination with Nab-Paclitaxel or Cisplatin[13,14]. However, most patients develop a resistance to Gemcitabine. Resistance mechanism can be versatile and may already be present before treatment or evolve throughout ongoing chemotherapy[15]. Possible resistance mechanisms include the downregulation of nucleoside transporters such as hENT1, modulation of various enzymes e.g. cytidine deaminase (CDA), secreted factors produced by cells in the TME and microRNAs[15]. Specifically, mutations affecting CDA in PDAC can significantly increase its activity, resulting in the breakdown and diminished efficacy of Gemcitabine[16].

Besides Gemcitabine, a combination of 5-fluorouracil (5-FU), leucovorin, irinotecan and oxaliplatin (FOLFIRINOX), is used for PDAC chemotherapy[15,17]. According to a meta-analysis by Zhang *et al.*[18] FOLFIRINOX shows better overall survival (OS) in metastasised pancreatic cancer compared to Gemcitabine mono- or combination therapy. Nevertheless, the higher levels of toxicity of this treatment limit the application to a selected patient group[18].

Hence, the selection of the optimal chemotherapy agents must be carefully evaluated, considering the stage of the disease as well as the patient's general health status.

1.4 Carcinogenesis of PDAC

Carcinogenesis is a complex multi-step process, involving mutations and epigenetic modifications of multiple genes regulating cell growth and tissue homeostasis[19]. Dysregulation of these critical pathways can lead to abnormal cell proliferation, survival and differentiation, ultimately promoting the development and progression of cancer [19].

In the exocrine pancreas, regeneration occurs in an injury context, e.g. in pancreatitis, which is an inflammation of the pancreas. Upon external stimuli such as stress, inflammation or tissue damage, acinar cells of the exocrine pancreas transdifferentiate to an epithelial, ductal-like phenotype in a process called acinar-to-ductal metaplasia in order to repair damaged tissue. During transition, acinar cells experience a progenitor-like stage which renders them vulnerable for proto-oncogene mutations (e.g. *KRAS*) resulting in a transformation to pancreatic intra-epithelial neoplasia (PanIN) which can ultimately lead to the development of pancreatic cancer (Figure 1) [6,20].

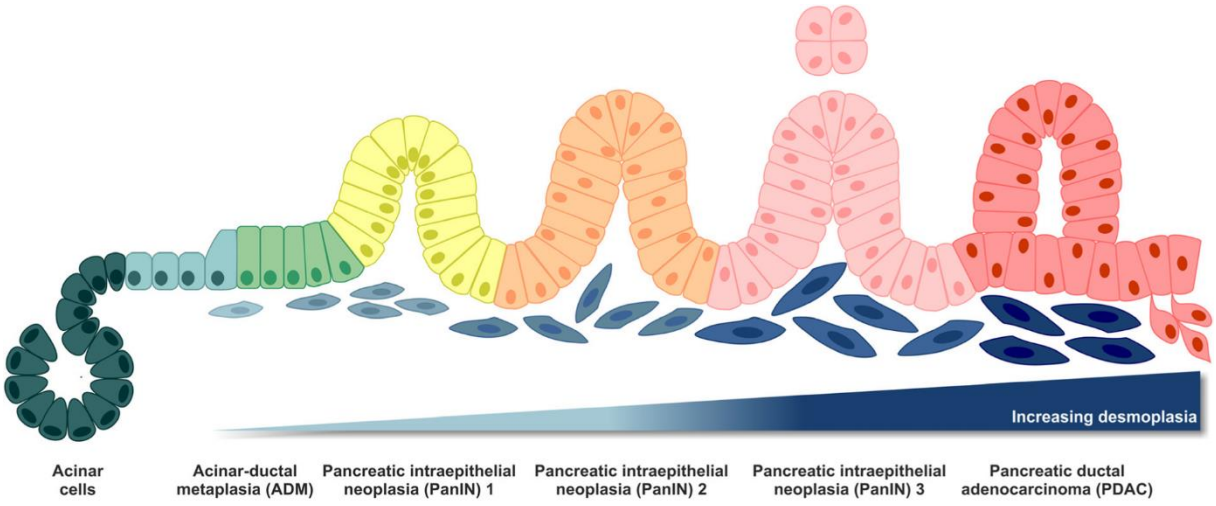

Figure 1 PDAC carcinogenesis. A sequential process from acinar cells to PDAC. Adapted from[6]. This figure is reproduced under the terms of the Creative Commons Attribution 4.0 International License (http://creativecommons.org/licenses/by/4.0/).

While the majority of PDAC is considered sporadic, there is an occurrence of up to 10 % of cases in individuals with a family history of the disease[20].

KRAS is the most important driver gene mutation in PDAC and is identified to be modified in 90 % of all patients[21]. Mutationally activated *RAS* genes, particularly *KRAS*, are found in various types of cancer, including PDAC and colorectal cancer[21]. Missense mutations in

cancer-associated *RAS* genes predominantly occur (98 %) at three specific mutational hot spots, namely glycine-12 (G12), glycine-13 (G13), or glutamine-61 (Q61), resulting in single amino acid substitutions[21].

KRAS is a small GTP-binding protein (GTPase), cycling between an active (GTP-bound) and inactive state (GDP-bound)[21]. When active, *KRAS* can control mitogenic processes such as the regulation of cell division. Mutations in *KRAS* render it constitutively active, leading to overstimulation of signaling pathways such as cell division which ultimately drives cancer growth[21].

Additionally, other common genetic alterations include the tumor suppressor genes cyclin-dependent kinase inhibitor 2A (*CDKN2A*), tumor suppressor protein 53 (*TP53*), and mothers against decapentaplegic homologue 4 (*SMAD4*)[22].

CDKN2A acts as a negative regulator of the cell cycle regulator *CDK4/6* and is inactivated in about 30 % of pancreatic cancer patients[23]. Its inactivation is accomplished through hypermethylation of the *CDKN2A* promoter, which contributes to the transcriptional silencing, ultimately resulting in uncontrolled cellular proliferation[24].

In 50-75 % of PDAC cases, *TP53* is inactivated through intragenic mutations combined with the loss of the second allele[25]. Particularly in the late PanIN stage, these *TP53* mutations lead to the loss of p53 function, providing a growth and survival advantage for cells with chromosomal aberrations[25].

SMAD4 plays a crucial role as a signal transducer in the tumor necrosis factor beta (TGF-β) signaling pathway. It is inactivated in about 55 % of pancreatic cancer cases, either through homozygous deletions or intergenic mutations and loss of the second allele[23,25]. This loss of *SMAD4* function provides a growth advantage for pancreatic cancer cells by eliminating the growth inhibitory signals mediated by TGF-β, particularly in the late PanIN stage[25].

Hence, the complex interplay of genetic alterations, such as *KRAS*, *CDKN2A*, *TP53* and *SMAD4*, plays a crucial role in driving the carcinogenesis of pancreatic cancer. Mutations in these genes promote uncontrolled cell division, provide growth advantages, and disrupt critical signaling pathways.

1.5 Metastases and the pre-metastatic niche in PDAC

PDAC is characterized by its tendency for early metastasis[6]. Metastatic seeding and outgrowth are associated with low survival and failure of therapy[26].

A review by Gumberger *et al.*[27] suggests that primary PDAC creates a favorable microenvironment in the liver, also referred to as pre-metastatic niche, which increases the likelihood of metastatic seeding[27]. This is in line with the “seed and soil” theory of metastasis, proposing that cancer cells (the seed) interact with favorable microenvironments in certain organs (the soil) throughout the body to promote non-random metastatic seeding and outgrowth[27].

Drivers of the pre-metastatic niche in PDAC are tumor-derived extracellular vesicles (EVs), soluble growth factors (e.g. GM-CSF), chemokines (e.g.CXCR2), cytokines and tumor-mobilized bone-marrow-derived cells (BMDC). Costa-Silva *et al.*[28] showed that PDAC-derived exosomes, taken up by Kupffer cells (KCs) in the liver, stimulate the release of TGF-β. Subsequently, this induces fibronectin (FN) production by activated hepatic stellate cells (HSCs) which promotes the recruitment and retention of additional BMDCs such as macrophages and neutrophils in the pre-metastatic niche[28]. Ultimately, these events establish a pro-inflammatory environment that supports metastasis.

1.6 What makes the liver particularly susceptible to metastasis?

The liver is considered the second most affected organ for metastasis in many cancers such as GI cancers, breast, prostate carcinomas, uveal melanoma, neuroendocrine tumors and sarcomas[29]. The reason for this organotropism is not fully understood but some assumptions are discussed in the following.

The process of metastasis from primary tumors to the liver involves several steps. Liver metastases occur when tumor cells undergo an epithelial-to-mesenchymal transition (EMT) and detach from their neighbouring cells in the primary tumor[29]. At the initial stage, tumor cells infiltrate the adjacent tissues, venules, capillaries, and the lymphatic system, gaining access to the circulation (a process known as intravasation)[30]. Upon entering the bloodstream, circulating tumor cells initiate the process of extravasation, exiting the blood vessels and infiltrating the liver[30]. Subsequently, tumor cells may demonstrate diverse behaviours, such as undergoing cell death, entering a dormant state, or actively proliferating. These processes contribute to the formation of micrometastases, which have the potential to progress into visible macrometastases within the liver (Figure 2)[29,30].

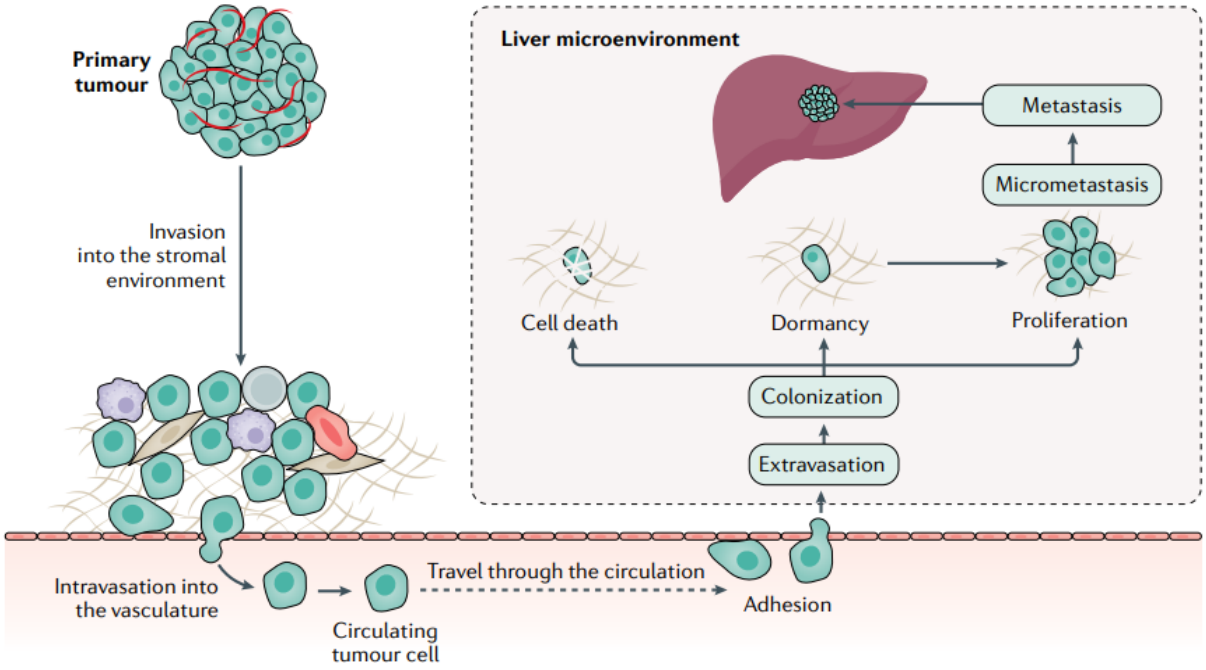

Figure 2 Tumor cell invasion into the liver. After EMT tumor cells are capable of travelling through the bloodstream. When reaching the liver, tumor cells either undergo cell death, stay dormant or proliferate. After proliferation, micrometastases form that further lead to the development of macrometastases, ultimately resulting in tumor formation. Figure taken from[30]. This figure is reproduced under the license number: 5596471261220.

The liver has a unique circulation with a dual blood supply system from the hepatic artery and portal vein that facilitates access for disseminated tumor cells. Additionally, the liver's slow blood flow and complex vascular structure create favorable conditions for interactions between tumor cells and liver tissue[29]. It has been described that liver sinusoidal endothelial cells (LSEC) facilitate the attachment and retention of tumor cells through the interaction of intracellular adhesion molecule 1 (ICAM-1) present on LSECs and lymphocyte function-associated antigen 1 (LFA-1) expressed by tumor cells[31]. Benedicto *et al.* showed that blocking ICAM-1 in LSECs reduced the adhesion and transmigration of tumor cells both in vitro and in vivo[31]. Moreover, co-culture experiments with tumor cells and LSECs revealed increased secretion of inflammatory mediators such as Interleukin-1 beta (IL-1β), Interleukin-6 (IL-6), Prostaglandin E-2 (PGE-2), tumor necrosis factor alpha (TNF-α) and ICAM-1 compared to monocultures, ultimately facilitating the infiltration of tumor cells during the process of liver metastasis[31].

Additionally, the regenerative machinery of the liver, involved in self-renewal and reconstruction, can be co-opted by signals such as cytokines or growth factors produced by tumor cells[29]. These signals promote the formation of intratumoral stroma and blood vessels within the liver, facilitating the support and nourishment of the tumor cells, thereby promoting their survival and growth in this organ[29]. Furthermore, its local immune suppression, due to its continuous exposure to inflammatory stimuli originating from the gut creates a favorable environment for tumor growth (further discussed in the following chapter, chapter 1.6.1)[29].

1.6.1 The establishment of the immunosuppressive microenvironment of liver metastasis

The entry of tumor cells into the liver causes an inflammatory response[32]. As part of this, the first line of defence that tumor cells encounter upon liver entry are LSEC, KC which are the liver-resident macrophages and natural killer cells (NK). These cells play a fundamental role in eliminating tumor cells by either secreting antitumorigenic factors such as TNF-α, or through the process of phagocytosis, resulting in the destruction of tumor cells[32].

Nevertheless, cancer cells that are trapped within the liver can exhibit resistance and even inhibit the anti-tumor microenvironment of the organ. This can be achieved through various factors, such as triggering interleukin-10 (IL-10) production[33]. Additionally, when cancer cells are clustered together, the inner cells are shielded from immune-defences originating from the body, allowing them to survive[33]. At this stage, immune cells such as KCs, neutrophils or monocytes together can built an immune-tolerant microenvironment through secretion of anti-inflammatory factors[30].

Liver metastases from lung, pancreatic, and colon carcinoma have been linked to the recruitment of immunosuppressive immune cells, specifically myeloid-derived suppressor cells (MDSCs)[30]. MDSCs are a diverse group of myeloid cells originating from the myeloid linage with immunoregulatory capabilities. They can give rise to macrophages, granulocytes and immature dendritic cells (DC)s. In the context of GI cancer, MDSCs are known to facilitate tumor-associated immune evasion, angiogenesis, and tumor metastasis[34]. A study by Gonda *et al*.[35] revealed that elevated levels of MDSCs in patients with GI cancer are linked to poorer clinical prognosis, advanced tumor stage, and higher mortality rates [34,35].

Other important cellular components that are found in established liver metastases and contribute to the growth and survival of the tumor are tumor-associated macrophages (TAMs),

which are discussed in chapter 1.6.3, cancer associated fibroblasts (CAFs) and cancer stem cells[33].

CAFs, a diverse group of activated fibroblasts, are a significant part of the tumor stroma[36]. They can originate from various cell types, such as fibroblasts, epithelial cells, endothelial cells, cancer stem cells, adipocytes, pericytes, or stellate cells[36]. Functionally, CAFs create a barrier both physically and metabolically by supplying ECM proteins, which diminishes the effectiveness of PDAC treatment. Additionally, they are believed to support the proliferation and invasion of tumors[36,37].

Taken together, liver metastases exhibit an immune suppressive microenvironment, characterized by the recruitment of immunosuppressive immune cells, specifically MDSCs, enabling tumor-associated immune evasion and fueling cancer progression.

1.6.2 Macrophage populations in the liver

Hepatic macrophages, which make up 90 % of the total macrophage population in the human body, play a crucial role in the immune response of the liver[38]. Based on their origin, macrophages can be divided into different subclasses (Figure 3).

KCs, named after Karl Wilhelm von Kupffer[39], are liver-resident, non-migrating macrophages depending on self-renewal[40]. They are the most abundant subclass of macrophages in the liver and are located within the hepatic sinusoids (Figure 3). Essential functions carried out by KCs are preserving the overall health of the liver through facilitating tissue recovery following injury and infections and triggering both innate and adaptive immune responses[38]. During homeostasis, KCs preserve an anti-tumorigenic environment by secretion of IL-10 and by interacting with hepatic regulatory T-cells (Tregs) [38].

In addition, the liver also houses liver capsular macrophages (LCM). LCMs originate from adult circulating monocytes and express typical macrophage as well as dendritic cell markers such as MHCII and CD11c[41]. LCM's main function is to detect peritoneal bacteria, thus recruiting neutrophils in order to reduce hepatic pathogen loads[42].

Upon injury, infection or loss of tissue resident macrophages, circulating monocyte-derived macrophages (moMs) are recruited [38,42]. MoMs, that originate from the bone marrow, have the ability to replace liver-resident macrophages such as KCs and assume similar functions once the inflammation has diminished[41,42].

Another class of macrophages are peritoneal macrophages (PM) that are recruited to the liver following injury and play a significant role during resolution of liver disease[38].

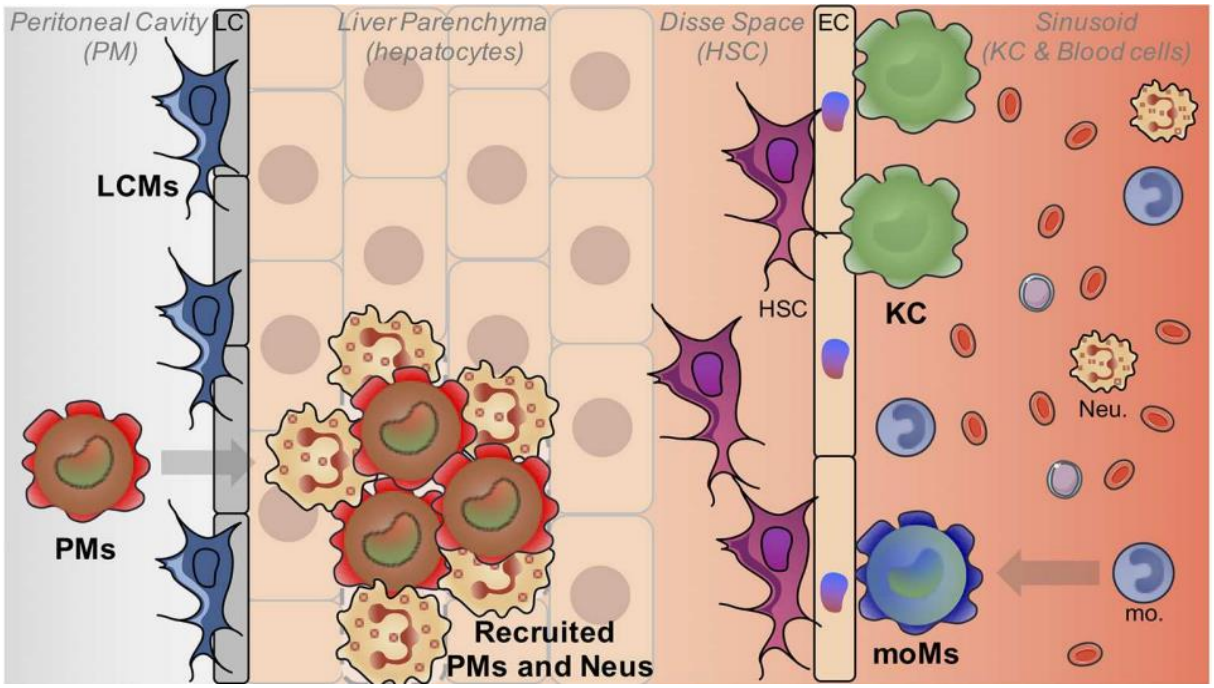

Figure 3 Macrophage populations in the liver. The liver comprises different macrophage subsets. Kupffer cells (KC) are tissue-resident and depend on self-renewal. Liver capsular macrophages (LCM) originate from adult circulating monocytes. Monocyte-derived macrophages (MoMs) originate from the bone marrow and are recruited to the liver upon injury. Peritoneal macrophages (PM) can be also recruited upon injury and play an important role during the resolution of liver disease. Figure taken from[38]. This figure is reproduced under the terms of Creative Commons Attribution License (CC BY).

1.6.3 Macrophage populations in liver metastases

When cancer cells successfully invade the liver and establish metastasis, they shape their TME including the macrophage populations, referred to as TAMs[43]. TAMs can exert pro- and anti-tumorigenic effects and their impact on tumor progression is strongly context-dependent.

Broadly, macrophages are capable of polarization into M1-type or M2-type macrophages. Generally, M1-type macrophages have pro-inflammatory functions and M1-type TAMs exhibit anti-tumorigenic effects[44]. In contrast, M2-type macrophages, are immunosuppressive and thus M2-type TAMs facilitate tumor growth[44]. However, the classification of TAMs into M1- or M2-type macrophages cannot be observed as a strict dichotomy but rather as a continuum[44].

M1- and M2-type TAMs can be distinguished by their surface receptors. For instance, CD206 is a cell surface marker for M2-type macrophages, while CD86 is present on M1-type

macrophages. Though, it has to be noted that some markers such as CD163, can be present on both types indicating the importance of considering a spectrum of markers when identifying and characterizing macrophages as M1- or M2-types[44].

Studies indicate that in primary PDAC, TAMs exhibiting the M2-type tumor-promoting phenotype, are associated with unfavourable prognosis and promotion of metastasis[43]. Xiong *et al.*[43] demonstrated that M2-type TAMs in primary PDAC have a notable impact on liver metastases by secreting TGF-β, which induces EMT in PDAC cells. Furthermore, Itatani *et al.*[45] showed a similar role of M2-type TAMs in colorectal cancer[45]. This process ultimately facilitates metastases[43]. In established liver metastases, TAMs were shown to have additional pro-tumorigenic functions like the promotion of tumor cell proliferation[42]. In addition, TAMs are able to create an immunosuppressive TME in liver metastases by expressing pro-angiogenic factors like VEGF and cell proliferation stimuli, such as IL-1β or IL-6. These factors can promote the proliferation of tumor cells[42].

1.7 The role of interleukin-6 (IL-6) in liver injury and metastases

The liver is a highly regenerative organ[44]. Liver regeneration is a well-coordinated process of tissue regrowth and is a crucial response to liver injury[46]. It consists of three distinct phases: priming, proliferation and termination. In the priming phase, certain cytokines such as TNF-α and IL-6 help sensitize hepatocytes to growth factors[46]. In the proliferative phase, growth factor stimulate hepatocytes to re-enter the G1 phase of the cell cycle and divide. Finally, in the termination phase, hepatocytes terminate proliferation to ensure the maintenance of normal liver mass and function[46].

1.7.1 The IL-6 signaling pathway

IL-6 is a cytokine comprising of four helices, which can signal through two different pathways. As shown in Figure 4, in the classical pathway, IL-6 binds to the membrane-bound IL-6 receptor (IL-6R) that is expressed on a limited number of cell types in the body including hepatocytes [47]. In order to activate downstream signaling, the IL-6/IL-6R associates with glycoprotein 130 (gp130), a transmembrane protein expressed on all human cell types, ultimately forming a heterocomplex. The IL-6/IL-6R/gp130 complex formation activates downstream signaling of the Janus kinase (JAK), eventually resulting in phosphorylation and activation of the transcription factor signal transducer and activator of transcription 3 (STAT3)[47,48].

It has been demonstrated that solely the whole complex of IL-6/IL-6R/gp130 can activate downstream signaling. However, membrane bound IL-6R was shown to be proteolytically cleaved at the cell surface by a disintegrin and metalloproteinase domain-containing protein 10 (ADAM10) or ADAM17, and released as soluble IL-6R (sIL-6R). The formation of sIL-6R has also been described as a result of alternative splicing[47–49]. The IL-6/sIL-6R complex can associate with gp130 and induce downstream signaling even in cells that do not express the IL-6R. This pathway is referred to as trans-signaling and can be inhibited by the formation of soluble gp130 (sgp130) [48].

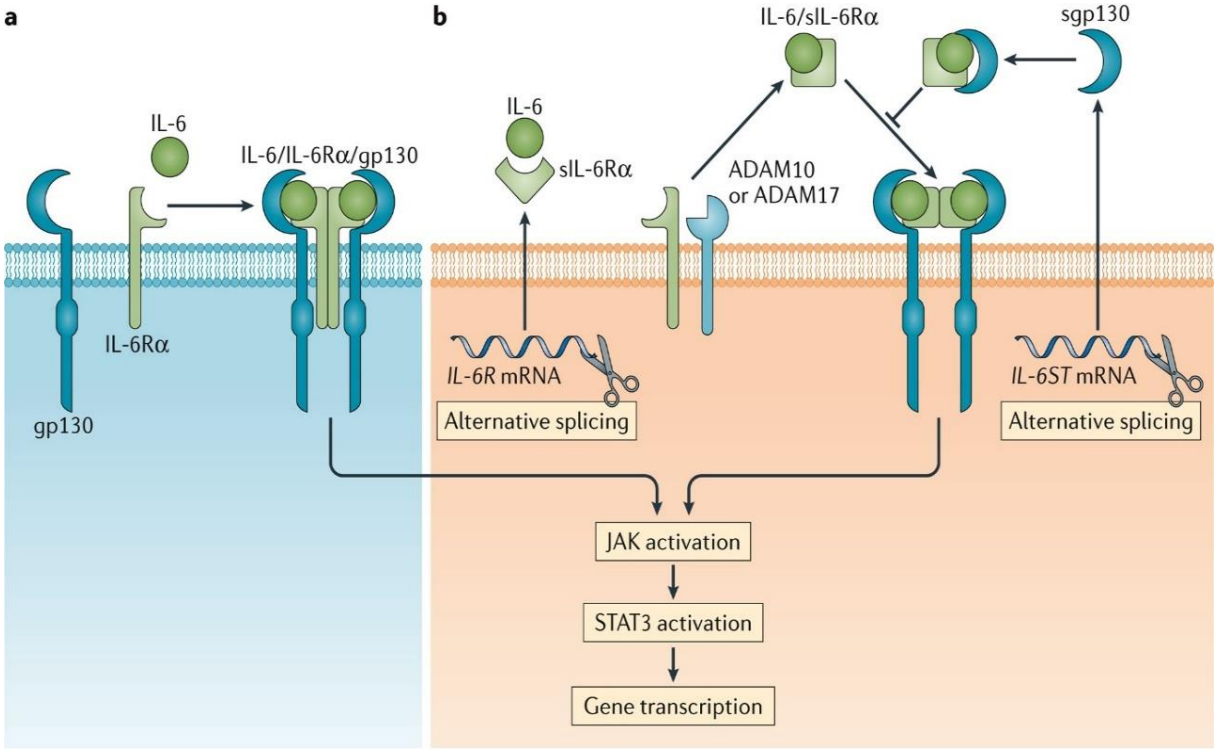

Figure 4 Canonical and trans-acting IL-6 signaling. a) In the canonical pathway IL-6 binds to the membrane bound IL-6 receptor that is only expressed on certain cell types such as hepatocytes. The IL-6/IL-6R complex associates with gp130 leading to the formation of a heterocomplex. Downstream signaling of JAK and STAT3 induces gene transcription. b) In the trans-signaling pathway IL-6 binds to soluble IL-6 receptor (sIL-6R), formed through alternative splicing. This complex associates with sg130 leading to the identical downstream signaling of JAK-STAT3. Gp130 is ubiquitously expressed on all human cell types, allowing IL-6 signaling to occur even if the cells do not express IL-6R itself. Picture taken from[48]. This figure is reproduced under the license number: 5596471498989.

1.7.2 The role of IL-6 in liver pathophysiology

The role of liver regeneration after injury has first been described by Higgins and Anderson in 1931[50]. Within their study, they successfully demonstrated a total regeneration of a rat liver after performing surgical removal of half of the liver (semi-hepatectomy)[50]. These findings marked the beginning of extensive research into liver regeneration[50]. In 1994 Kopf *et al.* showed in IL-6 knockout mice that the inflammatory acute phase response (APR) is impaired after liver injury or infection while its impact is relatively modest when exposed to lipopolysaccharide. Based on these findings, they conclude that IL-6 production, triggered by injury or infection, plays a crucial role as an in vivo distress signal that coordinates the functions of liver cells, macrophages, and lymphocytes[51].

Upon disruption of homeostasis such as tissue injury, infection or inflammation, the body undergoes a process referred to as APR with the liver being the main producer of acute phase proteins (APP)[52,53]. Hepatic Kupffer cells and the systemic release of pro-inflammatory cytokines such as IL-6, IL-8 and TNF-α serve as triggers for APR initiation[54]. Essential APPs, produced by hepatocytes are C-reactive protein (CRP), serum amyloid A (SAA) and haptoglobin (Hp)[52]. Typically, the APR involves a broad spectrum of pathophysiological responses such as fever, increased white blood cell count, hormonal changes, and depletion of muscle proteins[55]. These coordinated responses serve to mitigate tissue damage while promoting the repair process. Usually, the APR lasts for 24-48 hours before it is downregulated by stimuli like IL-10 or IL-4 cytokines[54].

Li *et al.* recently revealed that in response to liver injury, KCs secrete IL-6 which triggers nearby hepatocytes to undergo a reprogramming process, transforming them into so-called liver progenitor-like cells (LPLCs)[56]. LPLCs have the possibility to reprogram into proliferative hepatocytes and replace injured hepatocytes and colangiocytes[56].

Taken together, these findings highlight the importance of IL-6 signaling in liver regeneration[47,56].

1.7.3 The role of IL-6 in liver metastasis

While the classical IL-6 pathway is essential for acute-phase immunological response, the trans-signaling pathway has an important role in the TME by recruiting immune cells and promoting the production of pro-inflammatory cytokines[48]. It has been shown that elevated IL-6 levels correlate with advanced-stage disease, larger tumor size, and metastasis. Higher IL-

6 levels are also associated with poorer prognosis and resistance to therapy in various cancers including colorectal and pancreatic cancer [48].

Furthermore, tumor cell migration and metastases can ultimately lead to activation of APR and induction of APPs [57]. Previous results of the host group have shown an upregulation of APPs by hepatocytes in close proximity to tumor cells. However little is known about the effects.

1.8 Histopathological growth patterns of liver metastases

Different histopathological growth patterns (HGP)s of liver metastases can be identified originating from colorectal or pancreatic cancer and these patterns can be associated with survival outcome. According to the international consensus scoring guidelines, the two major HGPs are called replacement and desmoplastic/encapsulated type[58,59].

As the name suggest, in replacement type liver metastases, tumor cells seem to replace hepatocytes and utilize pre-existing sinusoidal blood vessels, to access their necessary nutrients and oxygen supply (Figure 5) in a process also described as vessel co-option[59]. In contrast, encapsulated liver metastases are characterized by a fibrotic capsule, consisting mainly of CAFs, immune cells and extracellular matrix[59,60]. The capsule separates tumor cells form their surrounding host-organ and tumors with a high degree of encapsulation are considered angiogenic[59,61] (Figure 5).

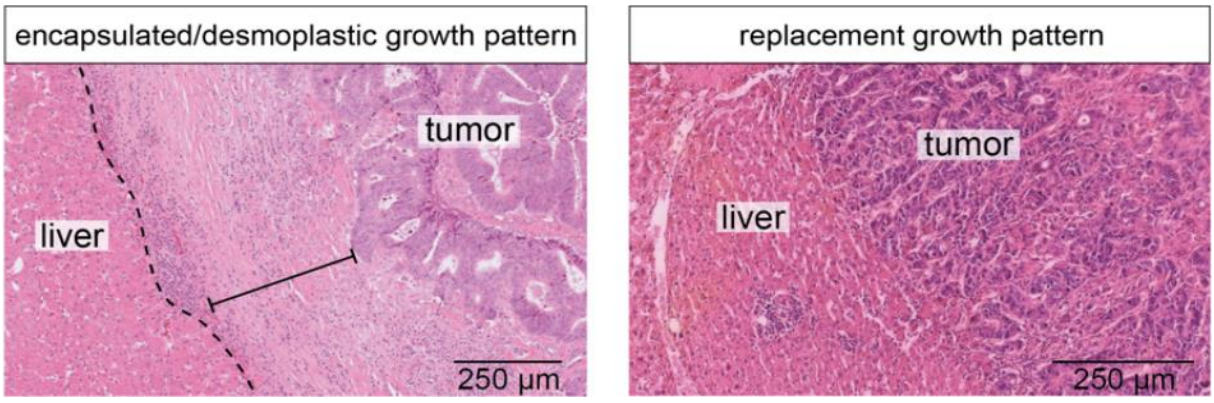

Figure 5 Histopathological growth patterns. In the encapsulated/desmoplastic growth pattern (left panel) the cancer cells are separated from the liver by a fibrotic capsule. In the replacement-type growth pattern liver cells are in direct contact to hepatocytes and appear to replace them. This figure is adapted from our manuscript [65].

As depicted in Figure 6, multiple retrospective studies have shown that patients with predominantly encapsulated liver metastases exhibit prolonged survival when compared to patients with predominant replacement-type liver metastases[59,61,62].

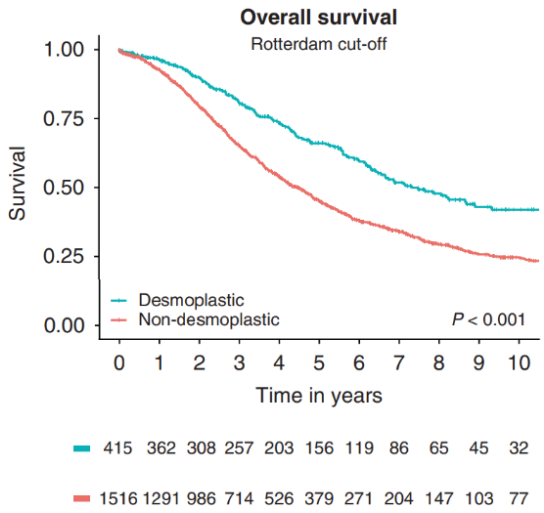

Figure 6 Overall survival rate of patients with colorectal cancer liver metastases according to the Rotterdam cut-off. Kaplan-Meier curves show a survival advantage in patients with desmoplastic histopathological growth patterns. The Rotterdam cut-off categorizes HGP into cases with 100% encapsulation and cases with mixed or pure non-encapsulated HGPs. Figure taken from [59]. This figure is reproduced under the terms of the Creative Commons Attribution 4.0 International License (http://creativecommons.org/licenses/by/4.0/).

While patients can present with metastases displaying more than one HGP, the "Rotterdam cut-off" categorizes them solely into two groups: cases with 100% encapsulation and cases with mixed or pure non-encapsulated HGPs[59].

Previously, the primary purpose of microscopic evaluation in the examination of resected liver specimens was to confirm the diagnosis and evaluate the extent of resection. However, in recent years, there has been a growing interest in studying specific tumor growth patterns in liver metastases and understanding their prognostic significance[59,63]. HGP are best studied in colorectal cancer liver metastases (CRLM) due to surgical resection being the standard care. However, multiple previous studies demonstrated that the prognostic value of scoring HGPs in liver metastasis extends beyond CRLM to encompass other types of liver metastases including pancreatic cancer liver metastases (PCLM)[59].

1.9 Aims and hypotheses

This project was structured around three distinct aims; aim one investigated encapsulated metastases, while aims two and three focused on replacement-type metastatic growth:

Firstly, we aimed to characterize the spatial distribution of stromal cells in the capsule of encapsulated CRLM. Predominantly encapsulated liver metastases have previously been found to be associated with favourable survival compared to predominantly replacement-type liver metastases[59]. However, the cellular composition and the origin of the capsule are poorly understood. Given the notable increase in the frequency of encapsulated growth patterns among patients who underwent neoadjuvant chemotherapy[64], we investigated the potential of chemotherapy to induce the formation of the fibrotic capsule in a CRLM mouse model.

Secondly, based on preliminary data by the host group, we hypothesized that IL-6 via APP production and consequent macrophage attraction might facilitate tumor invasion in liver metastases. To this end, we analyzed the impact of IL-6 blockage in a mouse model of PCLM. Specifically, we examined the macrophage count after IL-6 blockade and assessed the IL-6 signaling activity in hepatocytes by staining for phosphorylated STAT3 (pStat3).

Thirdly, the project aimed to establish and validate an in vitro model of physical interactions between hepatocytes and tumor cells. In replacement-type liver metastases, tumor cells seem to replace liver cells, however the mechanism is incompletely understood. To investigate whether the direct contact between tumor cells and hepatocytes triggers apoptosis as a possible mechanism of hepatocyte replacement, we established a co-culture model using pancreatic cancer cells and primary murine hepatocytes.

In this study, we hypothesized that chemotherapy could induce encapsulation in a CRLM mouse model. Additionally, we speculated that the perimetastatic injury response observed around liver metastases might be regulated by IL-6. Therefore, we assumed that inhibiting IL-6 would impact infiltrating macrophage numbers and reduce Stat3 signaling in hepatocytes. Lastly, we hypothesized that tumor cells induce apoptosis in hepatocytes upon close contact. This could serve as a potential mechanism of hepatocytes replacement in replacement-type liver metastases.

2. Material and Methods

2.1 Patients and ethics statement

Ethical approval for the work on human samples (#2019/ 01571 and #2021/06863-0, as well as #2018/1261-31 and 2019/05198) was granted by the Swedish National Ethical Review Board, *Etikprövningsmyndigheten*; informed consent for this retrospective study was waived. The participants received no monetary compensation.

Details regarding the KaroLiver cohort can be found our manuscript [65]. Briefly, the KaroLiver cohort includes 263 consecutive patients 18 years of age or older with CRLM operated on between 2012 and 2020 at Karolinska University, Huddinge, Sweden. All patients included in the main cohort underwent surgical resection of 1 or more CRLM at Karolinska University Hospital. The diagnosis of colorectal cancer metastases was confirmed histologically for all patients.

2.2 Mice and treatment

The Swedish Board of Agriculture approved the animal experiments via the regional ethics committee, Linköpingsdjurförsöksetiska nämnd (#217-2022 and # 22149-2022).

C57BL/6J mice obtained from Charles River were employed in all experiments. Included were both, female and male mice between 9-14 weeks of age. Mice were housed in specific-pathogen-free conditions at a 12 hour light/dark cycle at around 20 – 22 °C and fed standard chow.

Mice with CRLM were generated by performing ultrasound-guided (Vevo 3100 preclinical imaging system; Visualsonics, Toronto, Canada) intrahepatic injection of MC38 cells into the livers of C57BL/6 mice at a concentration of 10^5 cells. Presence of metastasis was confirmed using ultrasound imaging on day 15 post-injection. 24 tumor-bearing mice were then randomly assigned to receive either 5-FU (6 mg/kg) (Bio-Techne, #3257/50) and oxaliplatin (Oxa) (50 mg/kg) (Abcam, #ab141054) chemotherapy (n=14) or saline (n=10) on day 15 and 19. All mice were sacrificed 24 days after injection.

To generate mice with PCLM, ultrasound-guided intrahepatic injection (Vevo 3100 preclinical imaging system; Visualsonics, Toronto, Canada) of 10^5 KPC-T cells suspended in 50 µL sterile PBS was performed in C57BL/6J mice. PCLM growth was monitored by hepatic ultrasound on days 14 and 21. Tumor-bearing mice were randomly assigned to receive either MP5-20F3

(500 µg/mouse weekly) or sgp130Fc (60 µg/mouse weekly). Mice were sacrificed ten days after treatment onset.

Following the mice's sacrifice, the liver tissue was collected and placed in a 4 % formaldehyde solution (#1004965000, Sigma Aldrich) for incubation at room temperature for 24 hours. Subsequently, the tissue was transferred to 70 % EtOH for storage at 4 °C. The next step involved embedding the tissue in paraffin and then sectioning it at a thickness of 4-5 µm. It was ensured that the slide contained the largest visible tumor diameter.

2.3 Immunofluorescence staining on formalin-fixed paraffin-embedded sections

Formalin-fixed paraffin-embedded (FFPE) tissues of murine PCLM from IL-6 blocking antibody or isotype control treated mice were collected and used for immunofluorescence (IF) staining. Sections were cut at 4-5 µm thickness.

Prior to staining, sections were incubated at 60 °C for 1 hour. After deparaffinization in xylene (2x for 5 minutes each) and rehydration in a decreasing ethanol series (2x 99.5 %, 1x 95 %, 1x 70 %, 1x dH_2O for 5 minutes each), heat-induced epitope retrieval was performed using a 2100 Antigen Retriever (Aptum Biologics Ltd). Either DIVA decloaker (DV2004MX, BioCare Medical) or in-house prepared Tris-EDTA (pH 9) antigen retrieval buffer was used (Table 1). After cooling to room temperature (RT), slides were washed once with dH_2O and wash buffer which consists of TBS (10xTBS, Bio-Rad, #1706435) and 0.05 % Tween20 (PanReac AppliChem, #A4974) (TBST) for 5 minutes each. For blocking and permeabilization the sections were incubated in block-perm buffer (wash buffer supplemented with 1 % BSA (Sigma Aldrich, #A7960-100G), 10 % goat serum (Sigma Aldrich, #G9023), 0.1 % Triton X-100 (Sigma Aldrich, #MKBS6557V)) for 1 hour at RT. Then, samples were incubated with primary antibody diluted in block-perm buffer overnight at 4 °C in a humid chamber. Detailed information on the antibodies and respective retrieval buffers can be found in Table 1. The next day, slides were washed 3 times for 5 minutes using wash buffer and incubated with secondary antibody diluted 1:400 in block-perm buffer for 1 hour at RT. Subsequently, samples were washed with wash buffer and nuclei were counterstained for 15 minutes using DAPI (1 µg/ml, Thermo Fisher #121101) at a concentration of 0.001 mg/mL. Next, slides were mounted using Aqua-Poly Mount (Poly Sciences, #18606) and stored at 4 °C until imaging. Widefield and confocal images were acquired using a Nikon inverted confocal microscope with a Crest V3 spinning disk.

Table 1 Antibodies and retrieval buffers for immunofluorescence staining. The table gives detailed information about the primary and secondary antibodies used in immunofluorescence staining and their according retrieval buffer.

Primary Antibodies	Specificities	Provider	Reference	Dilution ratio	RB	Detection
F4/80	Mouse	Abcam	#ab6640	1:100	DIVA decloaker	Goat anti-rat AF647 (#A-21247)
pSTAT3	Human, Mouse, Rat, Monkey	Cell signaling	#9145	1:50	Tris-EDTA	Goat anti-rabbit AF647 (#A21245)

2.3.1 RNA in situ hybridisation

For the RNA in situ hybridisation (ISH), 4-5 µm FFPE patient samples from the KaroLiver cohort, were used. The markes Hs-COL1A1-T7, (401891-T7), Hs-DCN-T6 (589521-T6), Hs-THY1-T3 (430611-T3), Hs-FN1-T1 (310311-T1), Hs-PDGFRA-T2 (604481-T2) and Hs-SPP1-T5 (420101-T5) were utilized as probes and the RNAscope HiPlex12 Reagent Kit (488, 550, 650, 750) v2 (ACD, #324409) was employed following manufacturer's instructions. Samples were underwent a baking step at 60 °C for 1 hour, were then deparaffinized, and rehydrated followed by manual antigen target retrieval. Standard tissue pre-treatment conditions were applied. DAPI was employed to counterstain the nuclei and samples were mounted using ProLong Gold Antifade (#P36930). Wide field images were captured using a Kinetix sCMOS photometrics camera on a Nikon Eclipse Ti2 inverted confocal microscope with a Crest V3 spinning disk.

2.4 Genotyping Cas9

To establish a co-culture model, genotyping analysis on Gt(ROSA)26Sortm1.1(CAG-cas9*,-EGFP)Fezh/J mice was performed in order to identify individuals that express the Cas9-EGF construct, which leads to expression of the fluorescent protein, EGFP, facilitating visualization of the cells by fluorescence microscopy. DNA was isolated and PCR was performed using oIMR9020 AAG GGA GCT GCA GTG GAG TA as a wild-type and mutant forward primer, oIMR9021 CCG AAA ATC TGT GGG AAG TC as a wild-type reverse primer and 22163 CGG

GCC ATT TAC CGT AAG TTA T for mutant reverse. All primers are given in a 5' to 3' orientation. The PCR cycling steps consisted of an initial denaturation at 94 °C for 5 minutes, followed by 5 cycles of 25 seconds at 95 °C; 30 seconds at 64 °C; 60 seconds at 72 °C This was followed by 5 cycles of 25 seconds at 95 °C; 30 seconds at 62 °C; 60 seconds at 72 °C and another 5 cycles of 25 seconds at 95 °C; 30 seconds at 60 °C; 60 seconds at 72 °C. Samples were kept for 10 minutes at 72 °C followed by a cool down to 12 °C.

2.5 Cell culture

2.5.1 Cell line

The KPC-T cells were obtained by crossing the pancreatic cancer mouse model Pdx-1Cre, LSL-KrasG12D/+, LSL-Trp53R172H/+ (KPC) mice with B6.Cg-Gt(ROSA)26Sortm9(CAG-tdTomato)Hze/J to introduce the tdTomato marker. Cells were maintained in DMEM-F12 (Gibco, #11320033) with 10 % foetal bovine serum (FBS) (Sigma-Aldrich, #F2442) and 1 % Penicillin-Streptomycin (Pen-Strep) (Sigma-Aldrich, #P4333). Cultivation was performed at 37 °C and 5 % CO_2 in high humidity. Medium was exchanged every 2 to 3 days and cells were split for maintenance (95 % confluent) every 5 days at low concentration of 1:20 – 1:30 and discarded at passage 30. Cells used for experiment were split at 95 % confluent at higher concentration ranging from 1:5 – 1:15 (depending on the day of usage) with passage 10 to passage 26.

2.5.2 Primary hepatocyte isolation

Primary murine hepatocytes were obtained by two step-liver perfusion[66]. Mice were sacrificed by cervical dislocation under anaesthesia in 3-5 % isoflurane. The abdominal cavity was opened by incision and the liver and superior vena cava were revealed. Then, the vena cava was cannulated (BD, 0.5 mm BD Vacutainer® Valu-Set, 25G, #387425). 20 mL of pre-warmed sterile perfusion buffer (190 mg/ L mM EGTA (Sigma-Aldrich, #E3889), 2380 mg/ L HEPES (Gibco, #15630-056), HBSS mg/L no Calcium ($Ca2^+$) no Magnesium ($Mg2^+$)) (Gibco, #14175095) was slowly (2 mL/min) injected through the vena cava and the portal vein was cut in order to wash out blood, circulating cells and eliminate $Ca2^+$ (via EGTA) from the liver. For enzymatic digestion, Collagenase (Merck, 2.3 units/mg Liberase™ TM Research Grade, #5401119001) was diluted in 25 mL pre-warmed enzyme buffer (190 mg/ L mM EGTA, 2380 mg/L HEPES, HBSS 0.056 mg/L $CaCl_2$ x $2H_2O$ (Sigma-Aldrich, #10035-04-8) previously sterilized through filtration and prewarmed)) and perfused through the liver as previously. During the perfusion process, the portal vein was clamped manually and released (liver

swelling and relaxation) approximately 6 times in total allowing the buffers to reach all liver vasculature.

Next, the liver was carefully dissected and placed into a petri dish filled with enzyme buffer without liberase. The liver capsule was carefully ruptured using scissors. Through gently shaking the liver on ice, the hepatocytes were released into suspension, filtered through a 70 µm cell strainer (Corning, #352350) and transferred into a pre-cooled 50 mL Falcon tube. This process was repeated 5 - 7 times until the liver washing buffer appeared clear, indicating most hepatocytes were released.

2.6 Primary hepatocyte purification

For hepatocyte enrichment, the cell suspension was kept on ice and filled up to 50 mL with PBS + 10 % FBS (Sigma-Aldrich, #F2442). Next, the suspension was centrifuged at 300 x g for 5 minutes and the resulting cell pellet was resuspended in 20 mL PBS + 10 % FBS (Sigma-Aldrich, #F2442). In order to remove debris and to enrich for parenchymal cells, a low speed centrifugation at 41 x g with very low acceleration and break strength was performed for 3 minutes. The supernatant was removed and the resulting cell pellet was carefully resuspended in 10 mL PBS + 10 % FBS. Then the cell suspension was mounted on top of 10 mL Percoll mix (diluted 10:1 in 10x PBS) for density separation. The falcon was centrifuged at 1470 x g, acceleration and break = 1 for 20 minutes. Cells were collected at the interphase, transferred to a new tube and filled up to 20 mL with 20 mL PBS + 10% FBS (Sigma-Aldrich, #F2442). For the last experiment, no Percoll separation was performed to minimise the time between hepatocyte isolation and plating in order to increase cell viability. The falcon was centrifuged again at 300 x g for 5 minutes. Cells were counted and seeded in 8-well collagen-coated plates (Corning, #354630) at 2.4* 10^6 cells per well in 500 µl William' E medium (Gibco, #12551032) (+ 10% FBS (Sigma-Aldrich, #F2442), 1% Pen-Strep (Sigma-Aldrich, #P4333)) and in pre-coated collagen glass bottom dishes at 10.5* 10^6 per well. After 4 hours, the cells were washed with PBS, and the medium was replaced. For the last 2 experiments, only the medium was replaced in order to minimise hepatocyte loss through washing.

2.7 Co-culture

Primary hepatocytes were cultured for 24 hours in Williams' E medium (Gibco, #12551032) supplemented with 10 % FBS (Sigma-Aldrich, #F2442); 1 % Pen-Strep (Sigma-Aldrich, #P4333). Tumor cells (KPC-T) cells were pre-cultured in DMEM F:12 medium (Gibco, #11320033) supplemented with 10 % FBS (Sigma-Aldrich, #F2442); 1% Pan-Strep (Sigma-

Aldrich, #P4333). For tumor cell addition, KPC-T cells were washed with PBS, trypsinised (TrypLE™ Express Enzyme (1X), phenol red, Thermo Fisher scientific, #12605010), washed again in 20 mL PBS and centrifuged at 500 x g for 5 minutes. The resulting cell pellet was resuspended in 10 mL Williams' E medium (Gibco, #12551032) (+ 10% FBS (Sigma-Aldrich, #F2442); 1 % Pen-Strep (Sigma-Aldrich, #P4333)) and counted with the Invitrogen™ Countess™ 3 Automated Cell Counter. Next, the solution was centrifuged again at the same speed, the supernatant was discarded and the pellet was resuspended in one mL of Williams' E medium (Gibco, #12551032) (+ 10 % FBS (Sigma-Aldrich, #F2442); 1 % Pen-Strep (Sigma-Aldrich, #P4333). KPC-T were added on top of the primary hepatocytes at 8 x 10^4 tumor cells per well in 8 well collagen-coated plates (Corning, #354630) and in pre-coated Collagen Glass bottom dishes at 3,55 x 10^5 tumor cells per dish, followed by incubation at 37 °C, 5 % CO_2. After 4 hours, medium was exchanged and non-attached tumor cells removed. Co-cultures were cultivated for up to 72 hours in William's E medium (Gibco, #12551032).

2.7.1 Cell fixation

For cell fixation, cells were rinsed 3 times with 500 µL (8 well collagen-coated plates) or 2 mL (pre-coated Collagen Glass bottom dish) PBS, followed by the addition of 100 µL or 1 mL Formalin (Sigma-Aldrich, #1.00496.5000) incubated for 10 minutes at RT. Formalin was aspirated and each well was washed three times with 700 µL or 3 mL PBS. For storage, 400 µL or 2 mL of PBS were added to the Formalin-fixed cells and they were stored at 4 °C.

2.7.2 Immunofluorescence staining of Co-culture

Formalin-fixed cells from co-culture were used for IF staining. Cells were permeabilized with 0.1 % Triton X-100 (TritonTM X-10: Sigma Aldrich, #MKBS6557V) in PBS for 10 minutes. Next, cells were blocked for 30 minutes in PBS with 5 % BSA (A7960-100G, Sigma Aldrich) and 0.1 % Tween 20. Primary antibodies against Albumin (Thermo Scientific, #PA5-89332, 1:100) and cleaved Caspase 3 (Cell Signaling, #9664; 1:400) were diluted in PBS with 1 % BSA (A7960-100G, Sigma Aldrich) and 0.1 % Tween 20 (PanReac AppliChem, #A4974) and samples were incubated over night at 4 °C. On the next day, the samples were rinsed 3 times for 10 minutes in PBS, the secondary antibody (Thermo Fisher, Goat anti-Rabbit IgG (H+L) Highly Cross-Adsorbed Secondary Antibody, Alexa Fluor™ 647, #A21245) was diluted 1:400 and the samples were incubated for 1 hour at RT in the dark. Nuclei were counterstained for 15 minutes using DAPI (0.001 mg/ mL, Thermo Fisher #121101). Subsequently, slides were mounted using Aqua-Poly Mount (Poly Sciences #18606) and stored at 4 °C until imaging.

Widefield and confocal images were acquired using Nikon inverted confocal microscope with a Crest V3 spinning disk.

2.8 Data analysis

Cell detection, intensity value measurements and object classification were performed using QuPath version 0.4.3[67].

To analyze the macrophage count, positive cell detection was done using the DAPI channel and a threshold suitable for all images was chosen in order to detect the immunofluorescence signal of the marker F4/80.

Object classification was used in order to identify pStat3 positive cells within the invasion front and the liver parenchyma. For this, a training area was annotated and cell detection using the DAPI channel was used with default settings. Next, an object classifier was trained by manually annotating 25 cells of each group within the training area (pStat3 positive and pStat3 negative) for each image separately. Then, liver and invasion front were annotated manually, making sure to annotate an area where a minimal number of 1170 (liver) and 1879 (invasion front) cells per sample were analyzed with the specific object classifier for each image. To calculate the relative numbers of pStat3 positive cells, the total cell detections were summed for both the liver (n= 31851) and invasion front (n=32812) compartments, and similarly, the counts of pStat3 positive cells (n= 9564 (liver), n= 12596 (invasion front)) were aggregated. This enabled the determination of relative numbers by normalizing the count of pStat3 positive cells against the total cell count within each compartment.

To count viable hepatocytes (hepatocytes that are not floating in the medium) at different timepoints, an area of 90.000 μm^2 was annotated manually for one brightfield image and transferred to the others in order to have the same area for analysis for each timepoint. Next, hepatocytes were annotated manually for each timepoint (72 hours: n=3, 48 hours: n=3, 0 hours: n=3). The relative number of hepatocytes for each timepoint was calculated setting the number of cells for 0 hours to 100 %.

For co-culture analysis, single-cell measurement classifiers were used to identify different cell populations such as hepatocytes, tumor cells, clCasp3 positive hepatocytes and clCasp3 positive tumor cells. For the analysis of apoptosis in hepatocytes close to tumor cells, distances to annotations of different classes were measured.

For RNA ISH analysis, five regions of interest were selected. For each region, the desmoplastic capsule was annotated manually and expanded 1000 µm into the direction of the liver parenchyma and the tumor centre. Portal tracts were manually annotated and subtracted from the desmoplastic capsule and the liver parenchyma. Then, each annotation was divided in 25 μm^2 tiles. Within tiles, the mean intensities for each marker and the tile distances to the invasion front was measured.

All measurements were exported in a tabular format and analyzed in R, version 4.1.2 (2021-11-01). Data analysis was done with dplyr version 1.1.2, Rmisc version 1.5.1, stringr version 1.5.0 and caTools version 1.18.2. Package ggplot2 version 3.4.2 was used for visualization.

The statistical significance of differences between treated and control groups was assessed using the Wilcoxon rank sum test, considering p-values less than 0.05 as significant. To determine significant variations in the sum of relative numbers of pStat3 positive cells between the liver compartment and the invasion front, a 2-sample proportion test was employed, with p-values less than 0.05 considered as significant.

3. Results

3.1 Composition and formation of the fibrotic capsule in colorectal cancer liver metastases

Patients with predominantly encapsulated liver metastases are associated with a survival benefit compared to replacement-type liver metastases[59,62]. However, little is known about the underlying molecular mechanisms and the cellular composition of the protective capsule. We speculated that obtaining a deeper understanding of the cellular composition of the capsule could potentially reveal cues to its origin.

The fibrotic capsule shows stromal cell zonation in human colorectal cancer liver metastases

To characterize the spatial distribution of stromal cells within the capsule, we analyzed FFPE tissue samples obtained during routine pathological processing from patients with CRLM[65]. Stromally expressed mRNAs were analyzed by multiplex RNA ISH for *COL1A1* (Collagen Type I Alpha 1), *DCN* (decorin), *FN1* (fibronectin-1), *PDGFRA* (platelet derived growth factor receptor alpha), *SPP1* (osteopontin), and *THY* (Thy-1 cell surface antigen) (Figure 7 a). All markers were detected successfully (Figure 7 a-c).

By utilizing *COL1A1* as a major fibroblast marker, we demonstrate that the markers are specifically expressed within the fibroblast compartment, as they are detected in COL1A1-positive cells (Figure 7c). Furthermore, spatial analyses revealed a zonal expression of the capsule as *COL1A1, DCN*, *FN1* and *PDGFRA* were higher expressed in the outer part of the capsule (Figure 7 c-d). For quantitative analysis of the stromal markers the capsule was manually annotated and extended into the liver and tumor using QuPath [67]. Annotations were divided into 25 μm^2 tiles for intensity measurement of all markers, allowing comparison with our group's previous stromal marker results.

Taken together, the results indicate the zonated expression of stromal mRNA markers in the capsule. *COL1A1*, a fibroblast marker and *PDGFRA*, a marker for scar-associated mesenchymal cells that expand in fibrosis[68], are more abundantly expressed in the outer capsule. Hence, the results may point at the outer capsule being the place of active capsule formation.

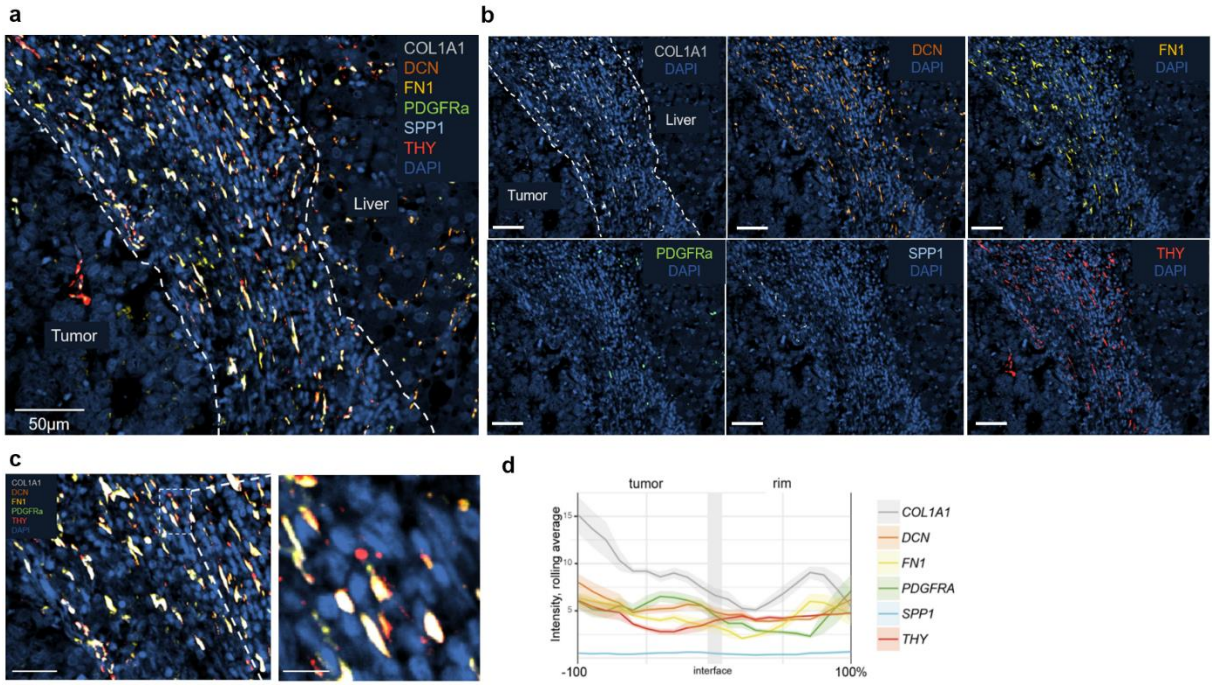

Figure 7 Multiplex in-situ hybridisation (ISH) and quantification for stromal markers COL1A1, DCN, FN1, PDGFRA, SPP1 and THY. a) All markers are combined. The dotted white line marks the inner and the outer part of the capsule. b) Each marker is shown separately together with the nuclear stain DAPI. The dotted white line marks the inner and the outer part of the capsule. The scaling bar indicates 50 µm. COL1A1, DCN, FN1 and PDGFRA show higher expression in the outer part of the capsule. c) COL1A1-positive cells (white) are positive for the stromal markers. On the left the scaling bar indicates 25µm, on the right the scaling bar indicates 12.5 µm. d) Intensities of stromal markers. The lines represent rolling averages, the areas represent 95% confidence interval. Figure 7 a, b and d is reproduced from our manuscript[65].

Chemotherapy promotes capsule formation in vivo

A recent study by Nierop *et al.*[64] discovered a preference towards encapsulated growth patterns in patients receiving pre-operative chemotherapy. Consistent with that observation, the host laboratory has detected a significant increase in the frequency of encapsulated growth patterns among patients who had undergone neoadjuvant chemotherapy compared to those who had not received treatment[65].

To functionally test the hypothesis that chemotherapy induces the encapsulated growth pattern, the host laboratory injected colorectal cancer cell line MC38[69] into C57BL/6 mice livers at a concentration of 10^5 cells and confirmed metastasis using ultrasound on day 15 after injection. Tumor-bearing mice were then randomly assigned to receive either chemotherapy (5-FU/Oxa) or saline. The substantial weight loss resulting from 5-FU/Oxa chemotherapy prompted the experiment's termination at the humane endpoint, nine days after treatment initiation.

In mice treated with 5-FU/Oxa, we identified zones of tumor cell necrosis, accompanied by the formation of a capsule that shared similarities with the capsules observed in human CRLM, while vehicle-treated mice more frequently showed replacement-type growth (Figure 8 a-c).

Alpha-smooth muscle actin (ASMA), a marker for fibroblast activation, is a characteristic marker of the fibrotic capsule in human metastases[59,65]. Hence, we performed immunofluorescence staining of ASMA on murine CRLM, to compare ASMA expression in human and murine metastases. As shown in Figure 8 d, the immunofluorescence staining was successful, showing expression of ASMA in the post-chemotherapy formed capsule. Notably, the liver was utilized as a negative control for ASMA, confirming its absence within the liver parenchyma (Figure 8 d).

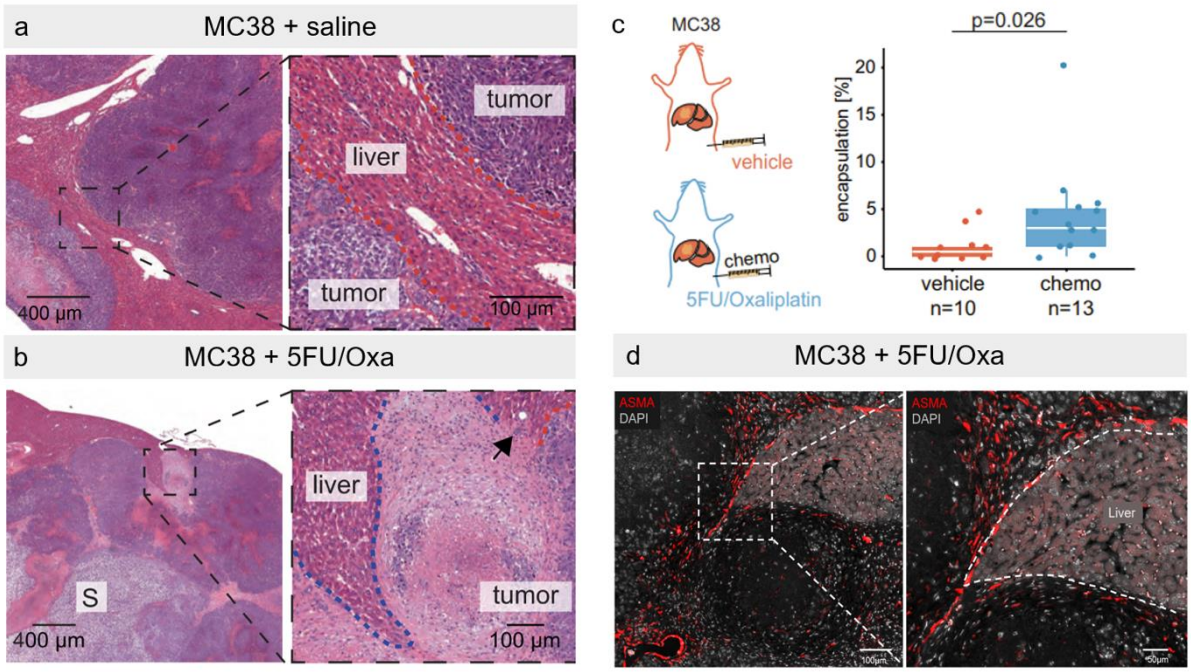

Figure 8 Alpha smooth muscle actin expression in the tumor liver interface of murine liver metastases after chemotherapy treatment. a) Hematoxylin & eosin (H&E) of mice carrying MC38 metastases treated with saline. b) Hematoxylin & eosin (H&E) of mice carrying MC38 metastases treated with 5-FU/Oxa. Red dashed line shows replacement, blue shows encapsulated growth. S: sarcomatoid growth. c) Mice (n=30) were injected with MC38 cells. On day 15, 24 mice had visible tumors on ultrasound and were included into chemotherapy (n=14) or saline (n=10) treatment groups (randomized). No tumor was visible on histology of one mouse in the treatment group. Box-and Whisker plots show the result from a two-sided Wilcoxon-test; median (line), interquartile range (box), minimum and maximum values within 1.5 times the IQR from the first and third quartiles (whiskers). d) Representative immunofluorescence for alpha-smooth muscle actin (ASMA, red) in an encapsulated metastasis after chemotherapy with 5-FU/Oxa treated mice (n=3). The dashed white box indicates the region of the zoom. The white dashed lines indicate the rim-liver border. Scaling bar indicates 100 µm (left) and 50 µm (right). Figure 8 a-d is reproduced from our mansuscript[65].

Collectively, our findings align with the prior observations made by Nierop *et al.*, indicating that chemotherapy triggers encapsulation.

In summary, we have explored the spatial distribution of stromal cells within the fibrotic capsule of CRLM. Through comprehensive analysis of stromal markers, we have revealed zonal expression patterns and demonstrated the potential of chemotherapy to induce capsule formation, reinforced by the presence of ASMA in post-chemotherapy capsules.

3.2 Effects of IL-6-blocking antibody treatment in murine pancreatic cancer liver metastases

In our second objective, we focused on investigating IL-6 signaling in murine PCLM samples. Therefore, the host group generated an IL-6 inhibition mouse model that allows us to study the functional role of IL-6 in liver metastasis. Mice were given IL-6-blocking antibodies and we assessed the success of the blockade by examining pStat3-positive cells, a readout for active downstream response to IL-6 after blockade. The reduction in the number of pStat3-positive cells would indicate the successful reduction of IL-6-mediated signaling.

Elevated levels of Stat3 phosphorylation in the perimetastatic liver of PCLM

Immunofluorescence staining of pStat3 was successful indicated by phosphorylation of Stat3 in the nucleus in hepatocytes across all samples, including both treated and non-treated with anti-IL-6 antibodies (Figure 9 a-d). Furthermore, throughout all the samples (treated and non-treated) we observed a heterogenous phosphorylation of Stat3 in all three compartments: liver, invasion front and tumor (Figure 9 b-d). Notably, visual assessment revealed a prominent signal of pStat3 particularly concentrated in hepatocytes around the invasion front within the liver (Figure 9 c). Hepatocytes can be distinguished by their size, as they typically exhibit larger dimensions compared to immune cells and endothelial cells. To confirm the visual observation, we performed relative cell quantification of cells positive for pStat3 in the invasion front as well as in the liver parenchyma. Annotations were performed manually within the liver and the invasion front, and cells were classified as pStat3 positive or negative with the help of a trained classifier in QuPath[67]. Relative quantification of the sum of pStat3 positive cells in both compartments (n=16 mice) indicates that there is a significant difference of pStat3 positive cells in the invasion and the liver (2-sample proportion test: X-squared = 501.59, df = 1, p-value < 2.2e-16). While in the invasion front, 38% of all identified cells exhibited pStat3 positivity, in the liver, only 30% of cells displayed pStat3 positivity (Figure 9 e).

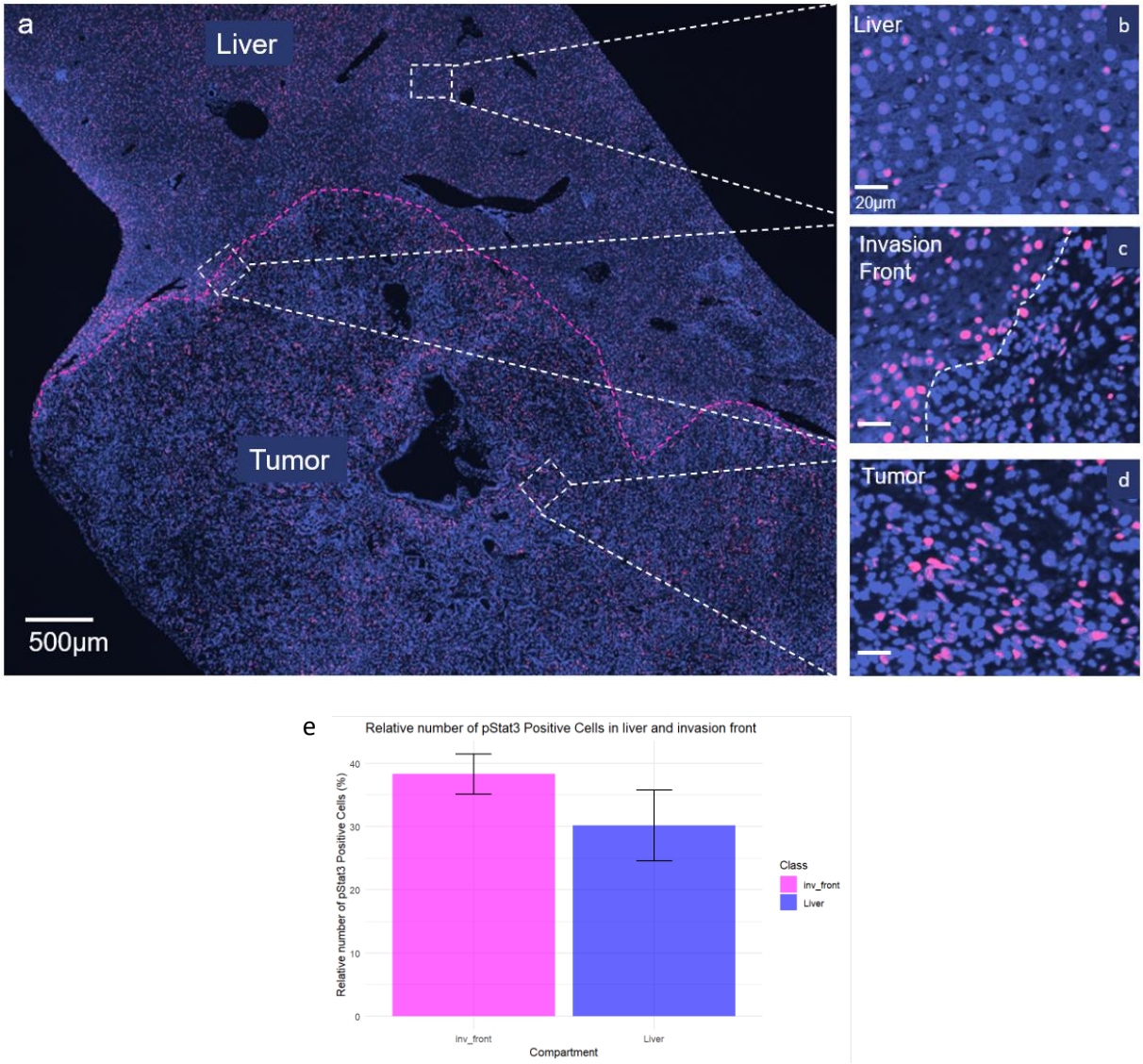

Figure 9 Stat3 phosphorylation in livers of PCLM-bearing mice. Representative visual representation of immunofluorescence staining for pStat3 (magenta) in liver of PCLM bearing mice. Nucleus counterstained with DAPI (blue). Dashed white line indicates the invasion front. Dashed white boxes and lines indicate the regions of the zoom image. Dashed magenta line indicates the metastases. a) Overview of liver with metastases. b) Nuclear pStat3 signal in hepatocytes within the liver. c) Nuclear pStat3 signal in hepatocytes near the invasion front. d) Nuclear pStat3 staining within the tumor. e) Bar plot showing the combined relative percentage of pStat3 positive cells in invasion front and liver (n=16 mice).

Taken together these results suggest that Stat3 signaling is activated in perimetastatic hepatocytes and, to a lesser extent, also in hepatocytes within the tumor-distant liver.

Stat3 phosphorylation in the liver of murine PCLM treated with IL-6-blocking antibodies remains unchanged

Next, we investigated the impact of IL-6 blockage on pStat3 abundance. Prior studies have suggested that IL-6 leads to upregulation of APPs in hepatocytes, which may have an impact on liver invasion and tumor aggressiveness in PCLM. To analyse the effects of IL-6 blockage, PCLM bearing mice received two distinct IL-6-blocking antibodies: MP5-20F3 and sgp130Fc. While the MP5-20F3 antibody is a neutralizing antibody that reacts with mouse IL-6, sgp130Fc explicitly targets the IL-6 trans-signaling pathway. This pathway is associated with the pro-inflammatory effects observed within the TME in cancer[47,70].

Subsequently, we analyzed the phosphorylation status of Stat3 in the liver and invasion front of murine PCLM that received IL-6-blocking antibodies and compared it to their respective isotype control.

As we hypothesized that we will detect less phosphorylation of Stat3 in mice treated with IL-6-blocking antibodies, we first quantified the number of pStat3 positive cells in the liver distant from the tumor.

When comparing treatment and control groups, visual assessment of the immunofluorescence images within the liver (Figure 10 a-d) did not reveal clear differences in nuclear pStat3. In line with this, staining quantification showed no significant difference (Wilcoxon rank sum test: W= 5, p-value = 0.571(MP5-20F3, rat IgG and sgp130Fc, human IgG Fc)) in the number of pStat3 positive cells between the IL6-blocked samples (MP5-20F3, sgp130Fc) and their isotype control samples (rat IgG and human IgG Fc, respectively) (Figure 10 e).

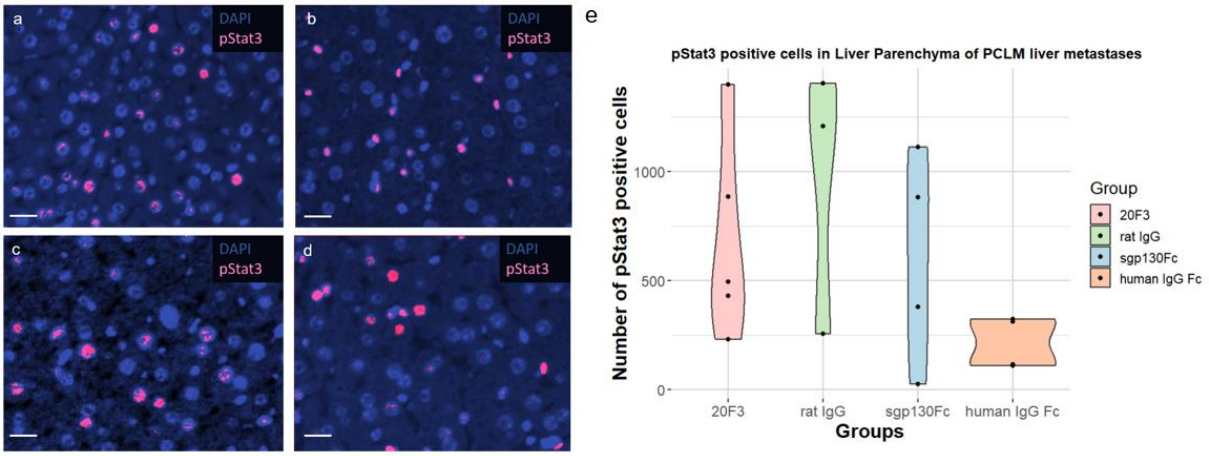

Figure 10 Phosphorylation of Stat3 in the tumor-distant liver of PCLM-bearing mice treated with Il-6 inhibitors. Visual representation of immunofluorescence staining for pStat3 (magenta). Nuclei are counterstained with DAPI (blue). A minimum of 1170 cells per sample was analyzed. Rat IgG corresponds to the isotype control of MP5-20F3 and human IgG Fc to sgp130Fc, respectively. Scaling bar indicates 20µm. Representative image for samples treated with a) the isotype control rat IgG (n=3), b) IL-6-blocking antibody MP5-20F3 (n=5), c) the isotype control human IgG Fc (n=4) and d) ILl-6-blocking antibody sgp130Fc (n=4). e) Violin plot depicts the average count of pStat3 positive cells among each group. Dots represent the average of each individual sample. Rat IgG corresponds to the isotype control of MP5-20F3 and human IgG Fc to sgp130Fc, respectively. Statistical testing (Wilcoxon rank sum test: W= 5, p-value = 0.571(MP5-20F3, rat IgG and sgp130Fc, human IgG Fc)) revealed no significant difference in pStat3 positive cell count in the liver parenchyma among treated versus control groups.

Next, we compared Stat3 phosphorylation in the perimetastatic liver between treated versus control groups. Again, as shown in Figure 9 c, we observed an accumulation of pStat3 positive cells in the perimetastatic liver in all four groups (Figure 11a-d). When performing quantitative analysis, we observed no significant difference (Wilcoxon rank sum test: W= 6, p-value = 0.786 (MP5-20F3, rat IgG and sgp130Fc, human IgG Fc)) in the phosphorylation of Stat3 among the treatment and control groups (Figure 11 e).

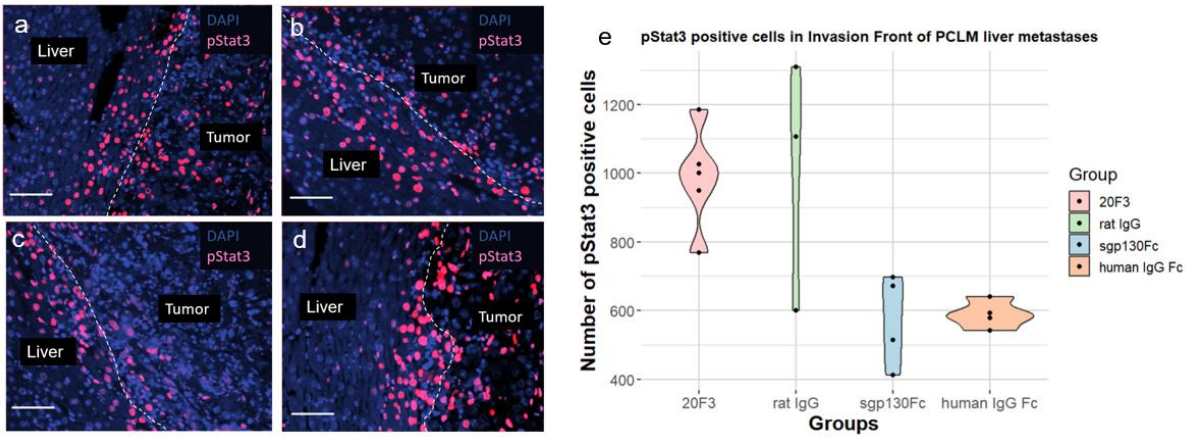

Figure 11 pStat3 positive cells in invasion front of PCLM bearing mice. Visual representation of pStat3 positive cells (red). Nucleus counterstained with DAPI (blue). A minimum of 1879 cells per sample was analyzed. White doted lines represent the tumor liver border (invasion front). Rat IgG corresponds to the isotype control of MP5-20F3 and human IgG Fc to sgp130Fc, respectively. Scaling bar indicates 50 µm. Representative image for samples treated with a) the isotype control rat IgG (n=3), b) IL-6-blocking antibody MP5-20F3 (n=5), c) the isotype control human IgG Fc (n=4) and d) IL-6-blocking antibody sgp130Fc (n=4). e) Violin plot depicts the average count of pStat3 positive cells among each group. Dots represent the average of each individual sample. Rat IgG corresponds to the isotype control of MP5-20F3 and human IgG Fc to sgp130Fc, respectively. Statistical testing (Wilcoxon rank sum test: W= 6, p-value = 0.786 (MP5-20F3, rat IgG and sgp130Fc, human IgG Fc)) revealed no significant difference in pStat3 positive cell count in the invasion front among treated versus control groups.

From these findings, we concluded that an accumulation of pStat3-positive cells occurs at the invasion front. However, our results indicate that IL-6-blocking antibody treatment did not have a significant impact on the phosphorylation status of Stat3. We did not detect a notable difference in pStat3 positive cell abundance between murine PCLM samples treated with IL-6-blocking antibodies and their corresponding isotype control samples.

Establishment of the macrophage staining

Encapsulation of liver metastases is typically accompanied by a dense immune cell infiltrate[59]. When we analyzed haematoxylin and eosin (H&E) stains from samples treated with IL-6-blocking antibodies (Figure 12 a), we similarly observed an immune cell infiltration in the perimetastatic liver. Macrophages are attracted by APPs and are a major immune determinant of the tumor microenvironment [71,72]. Thus, we asked if the number of macrophages observed within the tumor changed upon IL-6 inhibition.

To this end, we established a protocol for staining the general macrophage marker EGF-like module-containing mucin-like hormone receptor-like 1 (also known as F4/80) in murine PCLM tissue sections. As shown in Figure 12 b-d, the staining procedure was successful. Within the

liver parenchyma, KCs are located in the liver sinusoids and are connected to sinusoidal endothelial cells. This is shown in Figure 12 c, where F4/80 positively stained cells can be found in the perisinusoidal space that they occupy, thereby serving as an internal staining control. Moreover, upon visual examination, a pronounced F4/80 signal was noted in proximity to the invasion front (Figure 12 d).

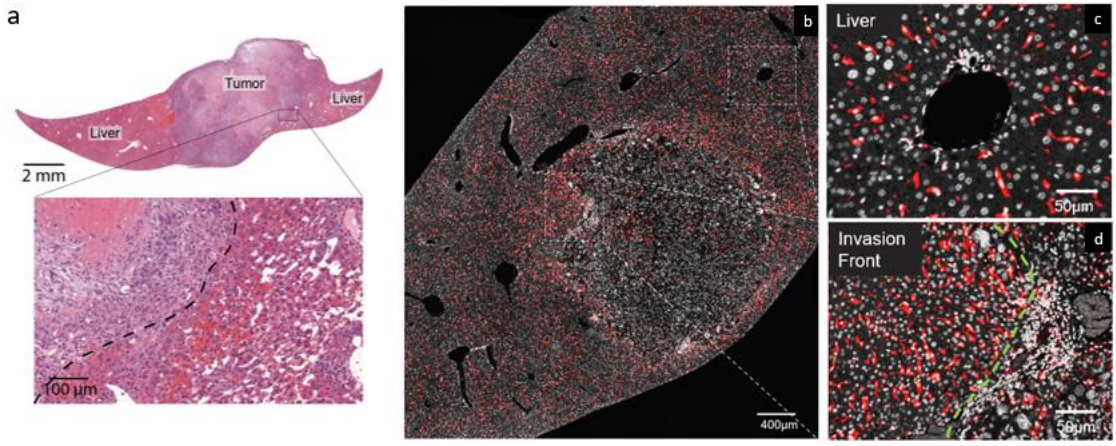

Figure 12 F4/80 expression in the tumor liver interface. a) Immune cell infiltration in haematoxylin and eosin staining (H&E) of IL-6-blocked samples. Black box indicates the region of the zoom. Dotted black line indicates invasion front. b) Representative immunofluorescence image for F4/80 (red) in PCLM replacement-type liver metastasis. F4/80 is shown together with the nuclear stain DAPI. Overview of liver metastases. The dashed boxes and lines indicate close up regions. c) F4/80 positive Kupffer cells in the liver. d) F4/80 positive macrophages close to the invasion front. The light green dashed line indicates the invasion front.

In conclusion, we established a staining protocol to successfully detect F4/80+ cells within the liver sinusoids, the invasion front and the tumor stroma. Moreover, a visually heterogeneity in the distribution of F4/80-positive macrophages was observed across all three compartments: liver, tumor, and invasion front, with the invasion front showcasing a particularly prominent signal of F4/80-positive cells.

No significant difference in macrophage count in PCLM from mice treated with IL-6-blocking antibodies

Next, we assessed the staining of macrophages after IL-6 blockade samples compared to the control group, to determine whether a significant disparity exists in the macrophage count within the tumor between the two groups. For this, we analysed mice treated with MP5-20F3 and sgp130Fc antibodies as before. We additionally used rat IgG and human IgG Fc as isotype control.

Immunofluorescence for F4/80 indicated successful macrophage staining within the tumor (Fig 13 a-d). Visual assessment revealed no obvious difference in macrophage count among IL-6-blocking antibody treated versus control groups within the tumor (Figure 13 a-d). To test whether the macrophage count within the tumor varied between treated versus control groups, we performed quantification analysis. For this, the whole tumor was annotated and positive cell detection was used to identify F4/80 positive macrophages, setting the same threshold (based on visual inspection) for all samples. In line with the visual assessment, quantification of F4/80 positive cells revealed no significant difference (Wilcoxon rank sum test: W = 11, p-value = 0.3929 (MP5-F20, rat IgG) and W = 14, p-value = 0.1143 (sgp130Fc, human IgG Fc)) in macrophage count among treated versus control samples groups, independent of the IL6-blocking antibodies that was used (Figure 13 e).

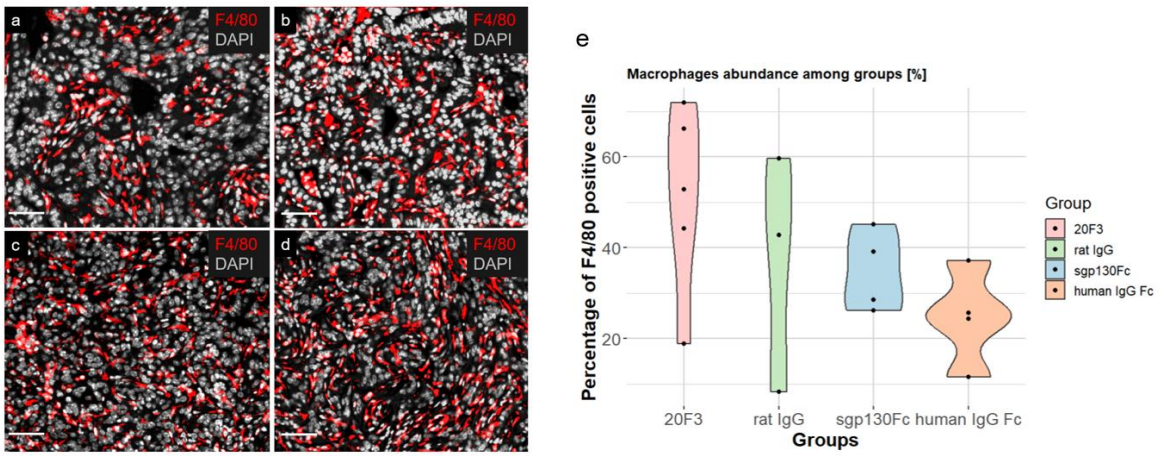

Figure 13 Macrophage abundance among IL6-blocking antibody treated versus control groups within the tumor. Visual representation of F4/80 positive cells within the tumor (red). Nucleus counterstained with DAPI (grey). A minimum of 27500 cells per sample was analyzed. Rat IgG corresponds to the isotype control of MP5-20F3 and human IgG Fc to sgp130Fc, respectively. Scaling bar indicates 50 µm. Representative image for samples treated with a) the isotype control rat IgG (n=3), b) IL-6-blocking antibody MP5-20F3 (n=5), c) the isotype control human IgG Fc (n=4) and d) IL-6-blocking antibody sgp130Fc (n=4). e) Violin plot depicts the percentage of F4/80 positive cells among each group. Dots represent the average of each individual sample. Rat IgG corresponds to the isotype control of MP5-20F3 and human IgG Fc to sgp130Fc, respectively. Statistical testing (Wilcoxon rank sum test: W = 11, p-value = 0.3929 (MP5-F20, rat IgG) and W = 14, p-value = 0.1143 (sgp130Fc, human IgG Fc)) revealed no significant difference in F4/80 positive cell count within the tumor among treated versus control groups.

Taken together, we did not observe a difference in macrophage count between IL-6 treated antibody versus control groups within the tumor.

In summary, our investigations have demonstrated that cells near the invasion front exhibit increased phosphorylation of Stat3 compared to cells in the tumor-distant liver. However, blockage of IL-6 had no impact on phosphorylation of Stat3 and macrophage count.

3.3 Inspecting the cellular interactions of tumor cells and hepatocytes

To address the third objective, we established a co-culture model. Hence, we aimed to determine whether tumor cells induce apoptosis in hepatocytes as a potential mechanism of cellular replacement.

For the co-culture experiments, we employed primary hepatocytes obtained from the mouse line Gt(ROSA)26Sortm1.1(CAG-cas9*,-EGFP)Fezh/J, which exhibit green fluorescent protein (GFP) expression specifically in their hepatocytes. Additionally, we utilized KPC-T cells that express tdTomato for the tumor cell component.

Establishment of a primary hepatocyte and murine PDAC cell line co-culture

To establish a tumor cell-hepatocyte co-culture system we isolated murine primary hepatocytes by two-step liver perfusion according to Jung *et al*[73].

For hepatocyte purification, we initially used Percoll density centrifugation to separate viable hepatocytes from dead and non-parenchymal cells[74]. However, a decrease in viability during this process was observed and it was omitted thereafter. This observation aligns with literature indicating that the use of Percoll can lead to a substantial reduction in the number of hepatocytes and pose a risk of impaired recovery[74]. As a result of omitting the Percoll step, we achieved, based on microscopic observation of cell culture density over time, improved hepatocyte recovery and viability. Furthermore, after performing albumin immunofluorescence staining on primary hepatocytes without Percoll, we observed uniform albumin expression across all hepatocytes, confirming the successful removal of non-parenchymal cells (Figure 14).

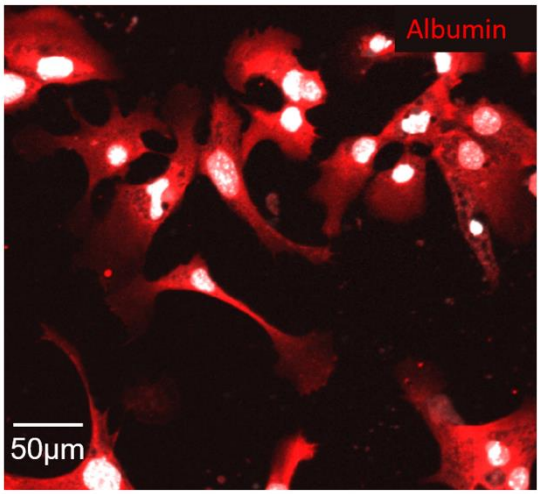

Figure 14 Albumin expression in primary hepatocytes. Primary hepatocytes isolated without Percoll expressing albumin.

The isolated and purified hepatocytes were cultivated on collagen-coated cell culture plates and co-cultured with KPC-T cells (Figure 15 a-d). Conducting long-term studies with primary hepatocytes in culture poses challenges due to their limited lifespan, cells are viable in 2D culture five to seven days[75]. Thus, in vitro cell morphology and culture density were investigated by light microscopy over time (Figure 15 b-d).

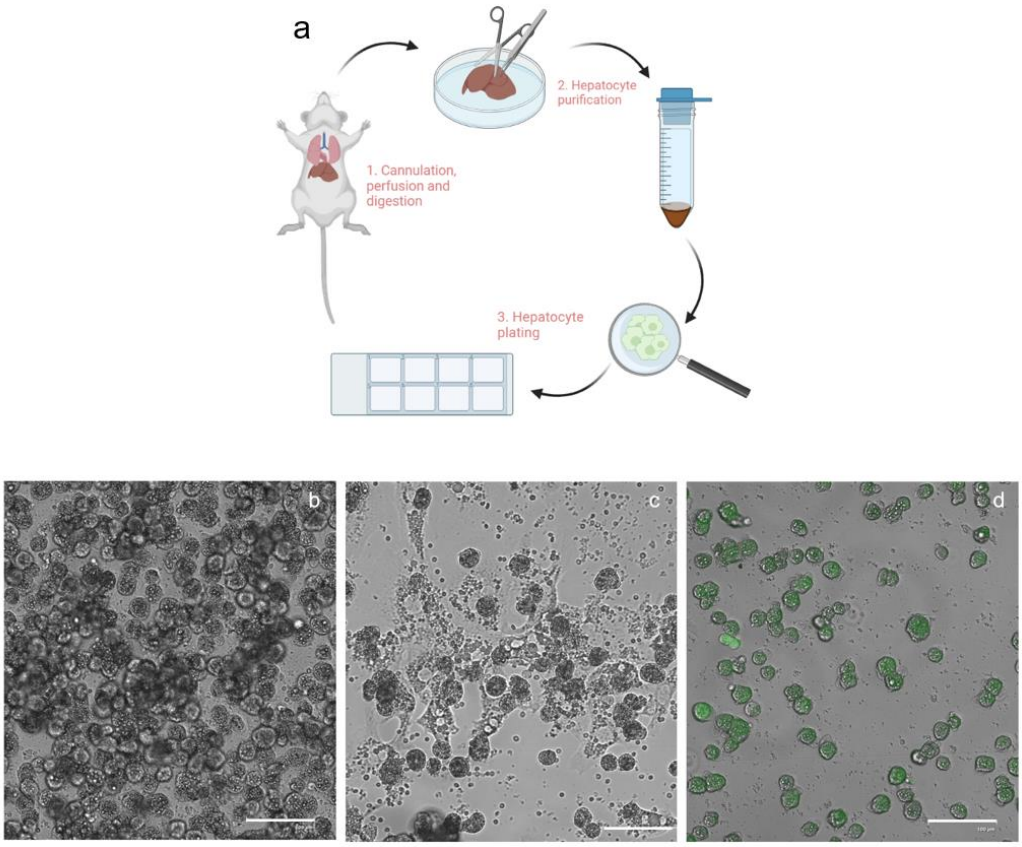

Figure 15 Primary murine hepatocytes can be cultured for 72h. a) Overview of the workflow of primary hepatocyte isolation and cultivation. Hepatocytes were isolated by two step liver perfusion. After hepatocyte purification, hepatocytes were plated on collagen matrix at 2.4 x 10^6 in 0.7 μm^2. Overview created with BioRender.com. Scaling bar indicates 100 µm. b) Hepatocytes immediately (0h) after isolation. Hepatocytes exhibit floating clusters of grey clouds, indicating their lack of attachment. c) Hepatocytes after 48 hours of isolation d) Hepatocytes (now marked green) after 72 hours of isolation.

After isolation, hepatocytes were spherical shaped with non-attached hepatocytes floating in clusters in the medium (Figure 15 b). After 48 hours of isolation, the hepatocytes displayed reduced cell viability, evident by a decrease in their numbers and the presence of cellular debris, indicating an ongoing process of cell death (Figure 15 c). Finally, 72 hours after isolation, extensive cell death was evident, characterized by increased cellular debris and minimal remaining attached cells (Figure 15 d). Thus, hepatocytes were not cultured for periods exceeding 72 hours from isolation.

We performed cell survival analysis over a 72-hour period, where cells were microscopically imaged and a designated area of 90.000 μm^2 was manually annotated. Subsequently, cells were counted manually, and relative proportions were computed. The assessment demonstrated that within 48 hours, over 50 % of the initially seeded hepatocytes underwent

cell death and were subsequently detached. After 72 hours post-isolation, around 17 % of the originally seeded hepatocytes were observed to remain attached within the collagen well. As anticipated, considering the significant cell loss during this timeframe, we initially plated a high number of hepatocytes (2.4 x 10^6 hepatocytes in a 0.7 μm^2 collagen well).

In conclusion, our experiments revealed that the cultivation of primary murine hepatocytes on a collagen-coated surface in a 2D setting can sustain less than 20 % of the initially attached cell population after 72 hours, indicating that they have to be seeded initially at a high concentration and can be cultured for a maximum of 72 hours.

No evidence of elevated hepatocyte apoptosis in proximity to tumor cells

Aggressive replacement-type liver metastases are characterized by direct physical interactions between hepatocytes and tumor cells. However, the mechanism is not fully understood. We hypothesized that cancer cells might induce apoptosis in hepatocytes to replace them. To assess whether tumor cells induce apoptosis in hepatocytes upon direct contact, we conducted staining of co-cultures for the apoptosis marker cleaved Caspase 3 (clCasp3) (Figure 16 a-f). Cleavage of Caspase 3 was observed in hepatocytes (Figure 16 b-c) successfully.

To investigate whether direct cell-to-cell contact between tumor cells and hepatocytes induces apoptosis, we calculated spatial distances between tumor cells and both apoptotic (clCasp3-positive) or non-apoptotic (clCasp3-negative) hepatocytes (Figure 16 d). No significant difference between the two groups was detected (Figure 16 d). Furthermore, Figure 16 e-f shows that during live-cell imaging, hepatocytes that were in close proximity to tumor cells did not undergo apoptosis. Hence, the observations from live cell imaging provide supporting evidence that hepatocytes in close proximity of tumor cells do not experience apoptosis induced by physical contact to tumor cells within the analyzed timespan.

Collectively, our findings suggest that the close interaction with tumor cells does not trigger apoptosis in hepatocytes in culture conditions.

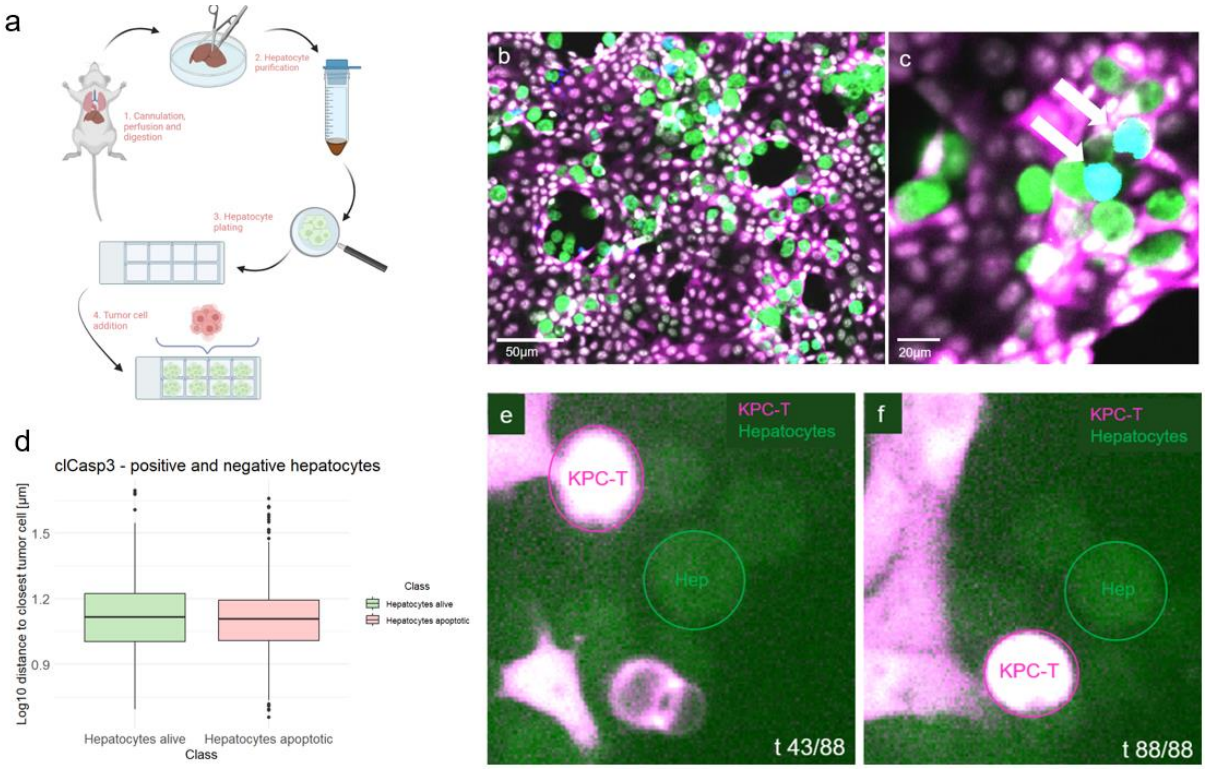

Figure 16 Physical contact with KPC-T cells does not induce apoptosis in hepatocytes. a) Overview of workflow of primary hepatocyte isolation, cultivation and addition of KPC-T cells. Overview created with BioRender.com b) Representative immunofluorescence image for clCasp3 co-culture staining. Cells were fixed 48 hours after addition of KPC-T cells. Hepatocytes are depicted in green, tumor cells in magenta and clCasp3 in blue. DAPI (grey) was used for counterstaining nuclei. c) Close up of apoptotic hepatocytes. White arrows indicate clCasp3 positive hepatocytes. d) Distance of apoptotic (clCasp3- positive) and non-apoptotic (clCasp3-negative) hepatocytes to the closest tumor cell. Boxplot represents the log10 distance. e-f) Live cell imaging of co-culture. Magenta circle indicated a KPC-T cell. Green circle indicates a hepatocyte. Of time (t 43-88) no cell death can be observed in hepatocytes close to a KPC-T cell.

4. Discussion

In my master's thesis project, I aimed to explore the role of the tumor cell niche in cancer and metastasis[76], with a specific focus on liver metastases arising from pancreatic cancer and colorectal cancer.

The first aim of this project was to characterize the stromal cells within the fibrotic capsule of encapsulated liver metastases, revealing a connection between the fibrotic capsule and the expression of specific stromal markers. Notably, cells positive for the fibroblast marker *COL1A1* demonstrated co-expression of *DCN*, *FN1* and *PDGFRA*. Cells expressing these stromal markers were locally enriched in the outer part of the capsule, close to the liver.

While *DCN* and *FN1* are known for their roles in regulating the assembly of the extracellular matrix and supporting other matrix proteins, playing crucial roles in tissue repair and remodelling processes[77,78], *PDGFRA* is primarily associated with its role in stimulating HSC proliferation, collagen production, and myofibroblast transformation[79]. Essentially, these markers have been demonstrated to be expressed during early fibrotic events[77–79].

As these markers show a zonal expression in the capsule, the findings propose a novel model hypothesis with active encapsulation locally occurring at the outer capsule. This has not been described before but would indicate that encapsulation may be driven by cellular signals from the tumor-surrounding liver rather than solely from tumor-derived signals. The host laboratory has finalised a manuscript on this hypothesis[65].

Furthermore, we propose that chemotherapy can trigger encapsulation, by weakening tumor cell fitness. Looking at tumor evolution, we propose that replacement-type growth serves as the inherent mode for successful and aggressive tumor invasion. This interpretation finds support in the fact that replacement-type growth is a prevailing feature in the majority of mouse models[59], including those employed in this study. Therefore, we suggest when tumor cells are weakened through e.g. chemotherapy and fail to induce the replacement-type growth, a hepatic injury reaction is triggered, resulting in the formation of a fibrotic capsule[65]. Our suggestion gains support from our mouse model, where we observed capsule formation after chemotherapy, as well as a recent study of growth patterns in the EORTC 40983 trial comparing neoadjuvant chemotherapy with immediate surgery [64]. In this study the authors conclude that preoperative chemotherapy induces changes in the histopathological growth patterns of CRLM.

In line with our results, the data propose that chemotherapy likely helps with encapsulation, possibly by affecting the health of tumor cells, which in turn reduces the likelihood of replacement growth.

Taken together, the findings propose a new hypothesis that the protective capsule observed in liver metastases from colorectal and pancreatic cancer is formed in the outer part of the capsule, facing the liver. In addition, in vivo chemotherapy and the associated weakening of tumor cells aggressiveness might hinder the capacity for replacement-type growth. Thus, we propose that capsule formation may be a result of local adaptation of the liver to metastatic growth triggered by failed tumor cell invasion.

In our second project, we investigated the blockade of IL-6 in PCLM. The cytokine IL-6 is a well-known regulator of liver damage and APP production[54,57]. Hence, we hypothesized that it might also play a role in the APP production in perimetastatic hepatocytes within the TME of liver metastases, potentially affecting tumor cell invasion. Therefore, IL-6 signaling was blocked in PCLM mice in vivo to comprehend the role of IL-6 and its effects on the TME.

Considering IL-6 blockage, mice were administered two different antibodies: MP5-20F3 and sgp130Fc. Both antibodies were shown to efficiently block IL-6 signaling in hepatocellular carcinoma (HCC)[47]. The fusion protein sgp130Fc explicitly targets the IL-6 trans-signaling pathway, which is associated with the pro-inflammatory effects observed within the TME of pancreatic, colon and liver cancer [47,70].

I investigated phosphorylation and nuclear translocation of the transcription factor Stat3 in murine PCLM samples, which becomes activated in response to IL-6. The activation of Stat3 in hepatocytes is primarily associated with IL-6[80]. A study by Lee *et al.*[81] demonstrated that IL-6 plays a key role in initiating the activation of Stat3 within hepatocytes. This activation, coupled with the elevated production of APPs such as SAA by hepatocytes, is a critical factor in the formation of a pro-metastatic niche in the liver. Their study also revealed that the IL-6-STAT3-SAA axis is involved in enhancing liver metastasis susceptibility and growth, as genetic disruption of IL-6-STAT3-SAA signaling effectively prevents the establishment of the pro-metastatic microenvironment and hampers liver metastasis[81].

Additionally, I conducted an investigation into the quantification of macrophage counts within IL-6-blocked samples compared to their respective control groups. A study by Zhou *et al.*[82] suggests that IL-6 plays a role in recruiting TAMs in HCC. They showed that overactivated YAP in HCC cells induces IL-6 expression, which in turn acts as a stimulant for the migration

of TAMs. This process promotes the recruitment of TAMs to the tumor microenvironment, ultimately influencing HCC progression and prognosis[82].

While we assumed to find a downregulation of Stat3 phosphorylation in hepatocytes as well as an alteration in macrophage count upon treatment with IL-6-blocking antibodies the results surprisingly revealed no significant difference for both among treatment and control groups in either of the analyzed compartments and with either of the two antibodies used.

This might be attributed to the possibility that the in vivo treatment did not effectively inhibit IL-6 signaling. To assess the potency of the IL-6-blocking antibodies used (sgp130fc, MP5-F20) the pancreatic cancer cell line KPC-T could be treated with either of the two antibodies. IL-6 levels could be measured before and after administration of the IL-6-blocking antibodies using an enzyme linked immunosorbent assay (ELISA) . In case the administered antibodies are successful in blocking IL-6 signaling, we would expect a significant reduction in the levels of IL-6 detected in the media after antibody treatment compared to untreated controls.

Nonetheless, an alternative hypothesis explaining the lack of reduction in Stat3 levels upon administration of IL-6 blocking antibodies could stem from the potential activation of Stat3 by other factors. Evidence suggests that another interleukin, IL-22, is also capable of activating Stat3 in the liver. A study by Jiang *et al.*[80] showed that IL-22 plays a crucial role in proliferation, cell survival and transformation from chronic hepatitis to HCC, with a potential involvement in sustaining Stat3 activation in hepatocytes. Hence, IL-22 could potentially compensate Stat3 activation in IL-6-blocked samples, explaining the Stat3 phosphorylation we observed in IL-6-blocked samples. Nevertheless, no comparable data is available in the context of PCLM. Hence, further experiments need to be done in order to validate this hypothesis and other cytokines such as IL-10 or TNF-α have been described to be able to activate Stat3 signaling independent of IL-6 as well[83,84].

In our third project we focused on cancer cell hepatocyte interaction. In replacement-type liver metastases tumor cells appear to replace liver cells, however the mechanism is not fully understood. Based on this, we hypothesized that cancer cells induce apoptosis in hepatocytes upon direct contact. In the co-culture model the apoptosis marker clCasp3 was stained by immunocytochemistry. As primary hepatocytes continuously undergo cell death throughout cultivation, it was expected to observe some hepatocytes being positive for the apoptosis marker clCasp3. In line with that about 80 % clCasp3+ hepatocytes were observed

72 hours after isolation. However, our findings do not confirm increased apoptosis in the hepatocytes close to tumor cells.

To this date there is no comparable literature available of pancreatic cancer cells and hepatocyte co-culture models that studied apoptosis. However, there is one study where colorectal cancer cell lines were co-cultured with hepatocytes. Rada *et al.*[85] conducted a study that examined hepatocyte displacement in CRLM. They observed cancer cells overexpressing TGFβ1 and Runt-related transcription factor 1 (RUNX1), leading to EMT in hepatocytes and enhanced apoptosis in hepatocytes close to tumor cells [85].

As we did not explore EMT in our co-culture setting and no comparable data exist, investigating EMT in a co-culture setting of pancreatic cancer cells and hepatocytes would represent an interesting avenue for future research. This approach could offer valuable insights into the observed discrepancy in hepatocyte apoptosis upon cancer cell contact, especially in comparison to the findings of Rada *et al.* who observed enhanced apoptosis in a co-culture model with colorectal cancer cells.

5. Conclusion and future perspectives

Taken together, this project was guided by three main objectives:

Firstly, we aimed to shed light on the origin of the fibrotic capsule and we propose that capsule formation may be a result of local adaptation of the liver to metastatic growth triggered by failed tumor cell invasion.

Secondly, we delved into the role of IL-6-blockage in PCLM, particularly assessing its potential influence on macrophage count and Stat3 phosphorylation and did not find evidence that in vivo administration of IL-6-blocking antibodies had an impact on macrophage count or phosphorylation of Stat3.

Lastly, our investigation into direct interactions between hepatocytes and tumor cells in a co-culture model did not support the hypothesis that hepatocyte-tumor cell contact induced apoptosis.

Continuing forward, there are several possibilities for future experiments that can help address unresolved questions:

Does IL-6 signaling have an impact on macrophage polarization?

TAMs are one of the most frequent immune cells that infiltrate PCLM, thus demanding significant attention towards their characterization and investigation[71]. Within the TME M2-type macrophages with an anti-inflammatory phenotype commonly predominate, which ultimately leads to tumor establishment and progression[71]. During my project, I initiated the development of a staining protocol to assess the macrophage polarization on IL-6-blocked PCLM samples using the M2-type marker CD206. The approach involves utilizing a general macrophage marker, CD68, to identify macrophages and then CD206 to classify M2-type macrophages. By quantifying the number of CD68/CD206-positive macrophages and comparing the counts between treated and untreated samples, we aim to determine whether the blockade of IL-6 has an impact on macrophage polarization. This analysis could provide valuable insights into the role of IL-6 in regulating TAM phenotype and its potential implications for tumor progression.

Do tumor cells activate Stat3 in hepatocytes, and if they do, is it through secretion or direct contact?

In tissue sections of murine liver metastases, hepatocytes in the perimetastatic liver showed enhanced phosphorylation of Stat3 (Figure 9 c). Thus, we hypothesized that tumor cells induce an active IL-6/Stat3 signaling response in hepatocytes.

We performed a preliminary experiment with Hyper-IL-6, acting as a control on our co-culture to help answer this open question. Hyper-IL-6 is a fusion protein constructed of IL-6 and its soluble receptor sIL-6R[49]. Hyper-IL-6 mimics the IL-6 trans signaling pathway by binding to gp130 and initiating downstream signaling. Contrary to the classical pathway, in the IL-6 trans signaling pathway, all cells are susceptible to IL-6 [49].

Preliminary results from the experiment suggest a higher number of pStat3 positive cells in the sample treated with Hyper-IL-6 and particularly in hepatocytes within the Hyper-IL6-treated samples, indicating that Hyper IL-6 works as a reliable control to induce Stat3 signaling.

Continuing forward, further experiments will elucidate whether cancer cells induce Stat3 signaling in hepatocytes through direct contact or the secretion of various factors by staining hepatocytes for pStat3 and measure tumor-hepatocyte distances.

Alternatively, it would be interesting to analyse whether IL-6 regulates Stat3 phosphorylation in perimetastatic hepatocytes. A straightforward strategy would involve subjecting co-cultures to IL-6-blocking antibodies, such as MP5-20F3 and sgp130Fc and to observe their impact on hepatocyte Stat3 phosphorylation. As sgp130Fc specifically blocks the trans-signaling pathway, by comparing the phosphorylation status of Stat3 between MP-20F3 and sgp130Fc we will gain valuable insight into the role of IL-6 trans-signaling in modulating Stat3 activation within the TME.

As an additional point to consider, the potential of Hyper-IL-6 to induce pStat3 should be noted. In light of this, the absence of pStat3 downregulation in IL-6-blocked samples from our prior experiments might suggest a potential failure in the treatment of the IL-6-blocking antibody, rather than an alternative activation through other cytokines like IL-22.

Which cytokine(s) contribute to inducing Stat3 activation independently of IL-6 blockage?

However, if the lack of Stat3 inhibition, despite successful IL-6 blockage, cannot be attributed to the inefficacy of the IL-6 blocking treatment, it raises the possibility that other cytokines

may be responsible for inducing Stat3 phosphorylation. In this context, the established co-culture system holds promise for providing further valuable insights.

As previously discussed, other cytokines such as IL-22 or IL-10 were shown to also induce Stat3 signaling in hepatocytes. To explore this further, we can utilize the co-culture system to investigate the cytokine release from tumor cells. This approach will enable us to identify the specific cytokines involved in Stat3 activation and gain a deeper understanding of the complex signaling network of tumor cell behaviour.

List of abbreviations

5-FU	5-fluorouracil
ADAM10	A Disintegrin and metalloproteinase domain-containing protein 10
APP	Acute Phase Proteins
APR	Acute Phase Response
ASMA	Alpha-smooth muscle actin
BMDC	Bone-marrow-derived cells
CDA	Cytidine deaminase
CDKN2A	Cyclin-dependent kinase inhibitor 2A
clCasp3	Cleaved Caspase 3
CRLM	Colorectal liver metastasis
CRP	C-reactive protein
CT	Computer tomography
ECM	Extracellular matrix
ELISA	Enzyme-linked Immunosorbent Assay
EMT	Epithelial and mesenchymal transition
EUS	Endoscopic ultrasound
EV	Extracellular vehicles
FBS	Feline bovine serum
FDA	Food and Drug Administration
FFPE	Formalin-fixed paraffin-embedded
FN	Fibronectin
GFP	Green fluorescent protein
GI cancer	Gastrointestinal cancer
Gp130	Glycoprotein 130
H&E	Haematoxylin & eosin
HCC	Hepatocellular carcinoma
HGP	Histopathological growth pattern
Hp	Haptoglobin
HSC	Hepatic stellate cells
IARC	International Agency for Research on Cancer
ICAM-1	Intercellular adhesion molecule 1

ISH	In situ hybridisation
JAK	Janus kinase
LCM	Liver capsular macrophages
IL	Interleukin
IL-6R	IL-6 receptor
ISH	In situ hybridisation
JAK	Janus-Kinase
KC	Kupffer cells
LFA-1	Lymphocyte function-associated antigen 1
LPLC	Liver progenitor-like cell
LSEC	Liver sinusoidal endothelial cells
MDSC	Myeloid-derived suppressor cell
moM	Monocyte-derived macrophage
MRI	Magnet resonance imaging
NK	Natural killer cell
OS	Overall survival
Oxa	Oxaliplatin
PanIN	Pancreatic intra-epithelial neoplasia
PCLM	Pancreatic cancer liver metastasis
PCLM	Pancreas cancer liver metastases
PDAC	Pancreatic ductal adenocarcinoma
Pen-Strep	Penicillin-Streptomycin
PET	Positron emission tomography
PGE-2	Prostaglandin E-2
PM	Peritoneal macrophages
pStat3	Phosphorylated Stat3
RT	Room temperature
SAA	Serum amyloid A
Sgp130	Soluble gp130
sIL-6R	Soluble IL-6R
SMAD4	Mothers against decapentaplegic homologue 4
STAT3	Signal transducer and activator of transcription 3

TAM	Tumor-associated macrophages
TGF	Tumor growth factor
TME	Tumor Microenvironment
TNF	Tumor necrosis factor
TP53	Tumor suppressor protein 53
Tregs	Regulatory T-cells

References

1. Arnold, M. *et al.* Global Burden of 5 Major Types of Gastrointestinal Cancer. *Gastroenterology* **159**, 335-349.e15 (2020).

2. Chen, J. L., Gurski, R. R., Takahashi, K. & Andersson, R. Gastrointestinal cancer metastasis. *Gastroenterology Research and Practice* Preprint at https://doi.org/10.1155/2012/415498 (2012).

3. Zhou, H. *et al.* Colorectal liver metastasis: molecular mechanism and interventional therapy. *Signal Transduction and Targeted Therapy* vol. 7 Preprint at https://doi.org/10.1038/s41392-022-00922-2 (2022).

4. Liu, Z., Gou, A. & Wu, X. Liver metastasis of pancreatic cancer: the new choice at the crossroads. *Hepatobiliary Surg Nutr* **12**, 88–91 (2023).

5. *Pancreas*. https://gco.iarc.fr/today (2020).

6. Orth, M. *et al.* Pancreatic ductal adenocarcinoma: Biological hallmarks, current status, and future perspectives of combined modality treatment approaches. *Radiation Oncology* vol. 14 Preprint at https://doi.org/10.1186/s13014-019-1345-6 (2019).

7. Siegel, R. L., Miller, K. D., Wagle, N. S. & Jemal, A. Cancer statistics, 2023. *CA Cancer J Clin* **73**, 17–48 (2023).

8. Wood, L. D., Canto, M. I., Jaffee, E. M. & Simeone, D. M. Pancreatic Cancer: Pathogenesis, Screening, Diagnosis, and Treatment. *Gastroenterology* vol. 163 386-402.e1 Preprint at https://doi.org/10.1053/j.gastro.2022.03.056 (2022).

9. Lowenfels, A. B. & Maisonneuve, P. Epidemiology and risk factors for pancreatic cancer. *Best Pract Res Clin Gastroenterol* **20**, 197–209 (2006).

10. Gnoni, A. *et al.* Carcinogenesis of pancreatic adenocarcinoma: Precursor lesions. *International Journal of Molecular Sciences* vol. 14 19731–19762 Preprint at https://doi.org/10.3390/ijms141019731 (2013).

11. Ansari, D., Gustafsson, A. & Andersson, R. Update on the management of pancreatic cancer: Surgery is not enough. *World Journal of Gastroenterology* vol. 21 3157–3165 Preprint at https://doi.org/10.3748/wjg.v21.i11.3157 (2015).

12. Wei, K. & Hackert, T. Surgical treatment of pancreatic ductal adenocarcinoma. *Cancers* vol. 13 Preprint at https://doi.org/10.3390/cancers13081971 (2021).

13. Principe, D. R. *et al.* The Current Treatment Paradigm for Pancreatic Ductal Adenocarcinoma and Barriers to Therapeutic Efficacy. *Frontiers in Oncology* vol. 11 Preprint at https://doi.org/10.3389/fonc.2021.688377 (2021).

14. Koltai, T. *et al.* Resistance to Gemcitabine in Pancreatic Ductal Adenocarcinoma: A Physiopathologic and Pharmacologic Review. *Cancers* vol. 14 Preprint at https://doi.org/10.3390/cancers14102486 (2022).

15. Zeng, S. *et al.* Chemoresistance in pancreatic cancer. *International Journal of Molecular Sciences* vol. 20 Preprint at https://doi.org/10.3390/ijms20184504 (2019).

16. Saiki, Y., Hirota, S. & Horii, A. Attempts to remodel the pathways of gemcitabine metabolism: Recent approaches to overcoming tumours with acquired chemoresistance. *Cancer Drug Resistance* vol. 3 819–831 Preprint at https://doi.org/10.20517/cdr.2020.39 (2020).

17. Wang, W. Bin *et al.* Recent studies of 5-fluorouracil resistance in pancreatic cancer. *World Journal of Gastroenterology* vol. 20 15682–15690 Preprint at https://doi.org/10.3748/wjg.v20.i42.15682 (2014).

18. Zhang, B. *et al.* The role of FOLFIRINOX in metastatic pancreatic cancer: a meta-analysis. *World Journal of Surgical Oncology* vol. 19 Preprint at https://doi.org/10.1186/s12957-021-02291-6 (2021).

19. Klaunig, J. E. Carcinogenesis. *An Introduction to Interdisciplinary Toxicology: From Molecules to Man* 97–110 (2020) doi:10.1016/B978-0-12-813602-7.00008-9.

20. Connor, A. A. & Gallinger, S. Pancreatic cancer evolution and heterogeneity: integrating omics and clinical data. *Nature Reviews Cancer* vol. 22 131–142 Preprint at https://doi.org/10.1038/s41568-021-00418-1 (2022).

21. Waters, A. M. & Der, C. J. KRAS: The critical driver and therapeutic target for pancreatic cancer. *Cold Spring Harb Perspect Med* **8**, (2018).

22. Ren, B. *et al.* Tumor microenvironment participates in metastasis of pancreatic cancer. *Molecular Cancer* vol. 17 Preprint at https://doi.org/10.1186/s12943-018-0858-1 (2018).

23. Dardare, J., Witz, A., Merlin, J. L., Gilson, P. & Harlé, A. SMAD4 and the TGFB pathway in patients with pancreatic ductal adenocarcinoma. *International Journal of Molecular Sciences* vol. 21 Preprint at https://doi.org/10.3390/ijms21103534 (2020).

24. Wu, C., Yang, P., Liu, B. & Tang, Y. Is there a cdkn2a-centric network in pancreatic ductal adenocarcinoma? *OncoTargets and Therapy* vol. 13 2551–2562 Preprint at https://doi.org/10.2147/OTT.S232464 (2020).

25. Polireddy, K. & Chen, Q. Cancer of the pancreas: Molecular pathways and current advancement in treatment. *Journal of Cancer* vol. 7 1497–1514 Preprint at https://doi.org/10.7150/jca.14922 (2016).

26. Majidpoor, J. & Mortezaee, K. Steps in metastasis: an updated review. *Medical Oncology* vol. 38 Preprint at https://doi.org/10.1007/s12032-020-01447-w (2021).

27. Gumberger, P., Bjornsson, B., Sandström, P., Bojmar, L. & Zambirinis, C. P. The Liver Pre-Metastatic Niche in Pancreatic Cancer: A Potential Opportunity for Intervention. *Cancers* vol. 14 Preprint at https://doi.org/10.3390/cancers14123028 (2022).

28. Costa-Silva, B. *et al.* Pancreatic cancer exosomes initiate pre-metastatic niche formation in the liver. *Nat Cell Biol* **17**, 816–826 (2015).

29. Clark, A. M., Ma, B., Taylor, D. L., Griffith, L. & Wells, A. Liver metastases: Microenvironments and ex-vivo models. *Exp Biol Med* **241**, 1639–1652 (2016).

30. Tsilimigras, D. I. *et al.* Liver metastases. *Nature Reviews Disease Primers* vol. 7 Preprint at https://doi.org/10.1038/s41572-021-00261-6 (2021).

31. Benedicto, A. *et al.* Liver sinusoidal endothelial cell ICAM-1 mediated tumor/endothelial crosstalk drives the development of liver metastasis by initiating inflammatory and angiogenic responses. *Sci Rep* **9**, (2019).

32. Brodt, P. Role of the microenvironment in liver metastasis: From pre- to prometastatic niches. *Clinical Cancer Research* vol. 22 5971–5982 Preprint at https://doi.org/10.1158/1078-0432.CCR-16-0460 (2016).

33. Vidal-Vanaclocha, F. The prometastatic microenvironment of the liver. *Cancer Microenvironment* vol. 1 113–129 Preprint at https://doi.org/10.1007/s12307-008-0011-6 (2008).

34. Farshidpour, M., Ahmed, M., Junna, S. & Merchant, J. L. Myeloid-derived suppressor cells in gastrointestinal cancers: A systemic review. *World J Gastrointest Oncol* **13**, 1–15 (2021).

35. Gonda, K. *et al.* Myeloid-derived suppressor cells are increased and correlated with type 2 immune responses, malnutrition, inflammation, and poor prognosis in patients with breast cancer. *Oncol Lett* **14**, 1766–1774 (2017).

36. Kobayashi, H. *et al.* Cancer-associated fibroblasts in gastrointestinal cancer. *Nature Reviews Gastroenterology and Hepatology* vol. 16 282–295 Preprint at https://doi.org/10.1038/s41575-019-0115-0 (2019).

37. Shinkawa, T., Ohuchida, K. & Nakamura, M. Heterogeneity of Cancer-Associated Fibroblasts and the Tumor Immune Microenvironment in Pancreatic Cancer. *Cancers* vol. 14 Preprint at https://doi.org/10.3390/cancers14163994 (2022).

38. van der Heide, D., Weiskirchen, R. & Bansal, R. Therapeutic Targeting of Hepatic Macrophages for the Treatment of Liver Diseases. *Frontiers in Immunology* vol. 10 Preprint at https://doi.org/10.3389/fimmu.2019.02852 (2019).

39. *Comparative Hepatology Opening Lecture*. http://www.comparative-hepatology.com/content/3/S1/S2.

40. Krenkel, O. & Tacke, F. Liver macrophages in tissue homeostasis and disease. *Nature Reviews Immunology* vol. 17 306–321 Preprint at https://doi.org/10.1038/nri.2017.11 (2017).

41. Blériot, C. & Ginhoux, F. Understanding the Heterogeneity of Resident Liver Macrophages. *Frontiers in Immunology* vol. 10 Preprint at https://doi.org/10.3389/fimmu.2019.02694 (2019).

42. Wen, Y., Lambrecht, J., Ju, C. & Tacke, F. Hepatic macrophages in liver homeostasis and diseases-diversity, plasticity and therapeutic opportunities. *Cellular and Molecular Immunology* vol. 18 45–56 Preprint at https://doi.org/10.1038/s41423-020-00558-8 (2021).

43. Xiong, C. *et al.* Tumor-associated macrophages promote pancreatic ductal adenocarcinoma progression by inducing epithelial-to-mesenchymal transition. *AGING 2021* (2020).

44. Wang, N. *et al.* Research trends in pharmacological modulation of tumor-associated macrophages. *Clin Transl Med* **11**, (2021).

45. Itatani, Y., Kawada, K. & Sakai, Y. Transforming growth factor-β signaling pathway in colorectal cancer and its tumor microenvironment. *International Journal of Molecular Sciences* vol. 20 Preprint at https://doi.org/10.3390/ijms20235822 (2019).

46. Tao, Y., Wang, M., Chen, E. & Tang, H. Liver Regeneration: Analysis of the Main Relevant Signaling Molecules. *Mediators of Inflammation* vol. 2017 Preprint at https://doi.org/10.1155/2017/4256352 (2017).

47. Rose-John, S. Interleukin-6 signalling in health and disease. *F1000Res* **9**, (2020).

48. Johnson, D. E., O'Keefe, R. A. & Grandis, J. R. Targeting the IL-6/JAK/STAT3 signalling axis in cancer. *Nature Reviews Clinical Oncology* vol. 15 234–248 Preprint at https://doi.org/10.1038/nrclinonc.2018.8 (2018).

49. Rose-John, S. The Soluble Interleukin 6 Receptor: Advanced Therapeutic Options in Inflammation. *Clin Pharmacol Ther* **102**, 591–598 (2017).

50. Al-Ghamdi, T. H. & Shafek Atta, I. *Efficacy of interleukin-6 in the induction of liver cell proliferation after hemi-hepatectomy: histopathologic and immunohistochemical study*. *Int J Clin Exp Pathol* vol. 13 www.ijcep.com/ (2020).

51. Kopf, M. *et al.* Impaired immune and APR. *Nature* **368**, (1994).

52. Gruys, E., Toussaint, M. J. M., Niewold, T. A. & Koopmans, S. J. Acute phase reaction and acute phase proteins. *J Zhejiang Univ Sci* **6 B**, 1045–1056 (2005).

53. Sander, L. E. *et al.* Hepatic acute-phase proteins control innate immune responses during infection by promoting myeloid-derived suppressor cell function. *Journal of Experimental Medicine* **207**, 1453–1464 (2010).

54. Todd, R. & Cocanour, C. APR. *The immunology of Trauma* 677–681 (2008).

55. Jain, S., Gautam, V. & Naseem, S. Acute-phase proteins: As diagnostic tool. *J Pharm Bioallied Sci.* (2011).

56. Li, L. *et al.* Kupffer-cell-derived IL-6 is repurposed for hepatocyte dedifferentiation via activating progenitor genes from injury-specific enhancers. *Cell Stem Cell* **30**, 283-299.e9 (2023).

57. Janciauskiene, S. *et al.* Potential Roles of Acute Phase Proteins in Cancer: Why Do Cancer Cells Produce or Take Up Exogenous Acute Phase Protein Alpha1-Antitrypsin? *Frontiers in Oncology* vol. 11 Preprint at https://doi.org/10.3389/fonc.2021.622076 (2021).

58. Tomlinson, J. S. *et al.* Actual 10-year survival after resection of colorectal liver metastases defines cure. *Journal of Clinical Oncology* **25**, 4575–4580 (2007).

59. Latacz, E. *et al.* Histopathological growth patterns of liver metastasis: updated consensus guidelines for pattern scoring, perspectives and recent mechanistic insights. *British Journal of Cancer* vol. 127 988–1013 Preprint at https://doi.org/10.1038/s41416-022-01859-7 (2022).

60. Garcia-Vicién, G. *et al.* Spatial Immunology in Liver Metastases from Colorectal Carcinoma according to the Histologic Growth Pattern. *Cancers (Basel)* **14**, (2022).

61. Höppener, D. J. *et al.* Histopathological Growth Patterns and Survival After Resection of Colorectal Liver Metastasis: An External Validation Study. *JNCI Cancer Spectr* **5**, (2021).

62. Fernández Moro, C., Bozóky, B. & Gerling, M. Growth patterns of colorectal cancer liver metastases and their impact on prognosis: A systematic review. *BMJ Open Gastroenterology* vol. 5 Preprint at https://doi.org/10.1136/bmjgast-2018-000217 (2018).

63. Zaharia, C. *et al.* Histopathological Growth Pattern in Colorectal Liver Metastasis and The Tumor Immune Microenvironment. *Cancers* vol. 15 Preprint at https://doi.org/10.3390/cancers15010181 (2023).

64. Nierop, P. M. H. *et al.* Preoperative systemic chemotherapy alters the histopathological growth patterns of colorectal liver metastases. *Journal of Pathology: Clinical Research* **8**, 48–64 (2022).

65. Fernández Moro, C. *et al.* An idiosyncratic zonated stroma encapsulates desmoplastic liver metastases and originates from injured liver. *Nat Commun* **14**, 5024 (2023).

66. Charni-Natan, M. & Goldstein, I. Protocol for Primary Mouse Hepatocyte Isolation. *STAR Protoc* **1**, (2020).

67. Bankhead, P. *et al.* QuPath: Open source software for digital pathology image analysis. *Sci Rep* **7**, (2017).

68. Ramachandran, P. *et al.* Resolving the fibrotic niche of human liver cirrhosis at single-cell level. *Nature* **575**, 512–518 (2019).

69. Schrörs, B. *et al.* MC38 colorectal tumor cell lines from two different sources display substantial differences in transcriptome, mutanome and neoantigen expression. *Front Immunol* **14**, (2023).

70. Schaper, F. & Rose-John, S. Interleukin-6: Biology, signaling and strategies of blockade. *Cytokine and Growth Factor Reviews* vol. 26 475–487 Preprint at https://doi.org/10.1016/j.cytogfr.2015.07.004 (2015).

71. Gao, J., Liang, Y. & Wang, L. Shaping Polarization Of Tumor-Associated Macrophages In Cancer Immunotherapy. *Frontiers in Immunology* vol. 13 Preprint at https://doi.org/10.3389/fimmu.2022.888713 (2022).

72. Cortese, N. *et al.* Macrophages in colorectal cancer liver metastases. *Cancers (Basel)* **11**, (2019).

73. Jung, Y., Zhao, M. & Svensson, K. J. Isolation, culture, and functional analysis of hepatocytes from mice with fatty liver disease. *STAR Protoc* **1**, (2020).

74. Horner, R. *et al.* Impact of Percoll purification on isolation of primary human hepatocytes. *Sci Rep* **9**, (2019).

75. Kim, Y. *et al.* Prolongation of liver-specific function for primary hepatocytes maintenance in 3D printed architectures. *Organogenesis* **14**, 1–12 (2018).

76. Wang, Q. *et al.* Role of tumor microenvironment in cancer progression and therapeutic strategy. *Cancer Medicine* vol. 12 11149–11165 Preprint at https://doi.org/10.1002/cam4.5698 (2023).

77. Baghy, K., Iozzo, R. V. & Kovalszky, I. Decorin-TGFβ Axis in Hepatic Fibrosis and Cirrhosis. *Journal of Histochemistry and Cytochemistry* **60**, 262–268 (2012).

78. Liu, X. Y. *et al.* Fibronectin expression is critical for liver fibrogenesis in vivo and in vitro. *Mol Med Rep* **14**, 3669–3675 (2016).

79. Ying, H. Z. *et al.* PDGF signaling pathway in hepatic fibrosis pathogenesis and therapeutics (Review). *Molecular Medicine Reports* vol. 16 7879–7889 Preprint at https://doi.org/10.3892/mmr.2017.7641 (2017).

80. Jiang, R. *et al.* Interleukin-22 promotes human hepatocellular carcinoma by activation of STAT3. *Hepatology* **54**, 900–909 (2011).

81. Lee, J. W. *et al.* Hepatocytes direct the formation of a pro-metastatic niche in the liver. *Nature* **567**, 249–252 (2019).

82. Zhou, T. *et al.* Interleukin-6 induced by YAP in hepatocellular carcinoma cells recruits tumor-associated macrophages. *J Pharmacol Sci* 89–95 (2018).

83. Wei, W. *et al.* Tumor necrosis factor-α induces proliferation and reduces apoptosis of colorectal cancer cells through STAT3 activation. *Immunogenetics* **75**, 161–169 (2023).

84. Hutchins, A. P., Diez, D. & Miranda-Saavedra, D. The IL-10/STAT3-mediated anti-inflammatory response: Recent developments and future challenges. *Brief Funct Genomics* **12**, 489–498 (2013).

85. Rada, M. *et al.* Cancer Cells Promote Phenotypic Alterations in Hepatocytes at the Edge of Cancer Cell Nests to Facilitate Vessel Co-Option Establishment in Colorectal Cancer Liver Metastases. *Cancers (Basel)* **14**, (2022).